Anharmonic oscillator modeling of nonlinear susceptibilities and its application to conjugated polymers

Akira Takahashi and Shaul Mukamel
Department of Chemistry, University of Rochester, Rochester, New York 14627

Molecular optical susceptibilities are calculated by deriving equations of motion for the single electron reduced density matrix, and solving them using the time dependent Hartree–Fock (TDHF) approximation. The present approach focuses directly on the dynamics of the charges in real space and completely avoids the tedious summations over molecular eigenstates. It further maps the system onto a set of coupled harmonic oscillators. The density matrix clearly shows the electronic structures induced by the external field, and how they contribute to the optical response. The method is applied to calculating the frequency-dispersed optical susceptibility $\chi^{(3)}$ of conjugated linear polyenes, starting with the Pariser–Parr–Pople (PPP) model. Charge density wave (CDW) like fluctuations and soliton pair like local bond-order fluctuations are shown to play important roles in the optical response of these systems.

I. INTRODUCTION

Recently, there has been increasing interest in the nonlinear optical properties of π-conjugated polymers, which are good candidates for optical devices because of their large nonlinear optical susceptibilities.[1-5] The nonlinear optical response of conjugated polymers is closely connected to some fundamental theoretical problems of one-dimensional systems such as strong electron correlations,[6] and the roles of exotic elementary excitations (solitons or polarons).[7] Furthermore, they are ideal model systems for studying exciton confinement effects in nanostructures.[8]

The frequency dispersion of nonlinear optical polarizabilities provides an important spectroscopic tool. A variety of third order techniques such as third harmonic generation (THG), two photon absorption (TPA), and four wave mixing result in a detailed microscopic probe of electronic and nuclear dynamics. These spectra are traditionally calculated using multiple summations over the molecular excited states.[9] However, this method has some serious limitations since it requires the computation of all the excited states in the frequency range of interest, as well as their dipole matrix elements. These computations pose a very difficult many-body problem, particularly since electron correlations are very important in low-dimensional systems such as π-conjugated polymers. Large scale numerical full configuration interaction calculations show that nonlinear optical polarizabilities are very sensitive to electron correlations.[6] This rigorous approach can be applied in practice only to very small systems (so far polyenes with up to 12 carbon atoms have been studied) because of computational limitations. Conjugated polyenes are characterized by an optical coherence length, related to the separation of an electron-hole pair of an exciton, which is typically $\sim$40 carbon atoms for polydiacetylene.[8] It is essential to consider systems larger than the coherence length in order to account for the scaling and the saturation of nonlinear susceptibilities with size.[8,10] Thus, several authors calculated the excited states in the independent electron approximation,[11-14] or by using configuration interaction including only single electron-hole pair excitations.[15] This method can be carried out for larger systems. However, it is valid only when correlation effects are weak, which is not the case here.[16] Additional difficulty with the sum over states method is the need to perform tedious summations over excited states. This forces us to work with small systems, or to truncate the summations, which again limits the accuracy for large systems. The sum over states method describes optical processes in terms of the excitation energies and transition dipole moments. These quantities provide very little physical insight regarding the optical characteristics of π-conjugated polymers, and do not directly address questions such as what kind of correlation is important, or how characteristic elementary excitations such as solitons affect the optical response. The synthesis of new optical materials calls for simple guidelines (structure-property relations)[17] which should allow us to use chemical intuition to predict effects of geometry and various substitutions on the optical susceptibilities. The sum over states method does not offer such simple guidelines, even when it does correctly predict the optical susceptibilities.

An alternative view of optical response may be obtained by abandoning the eigenstate representation altogether, and considering the material system as a collection of oscillators. It is well established that as far as the linear response is concerned, any material system can be considered as a collection of harmonic oscillators.[18] In fact, the term "oscillator strength" of a transition is based on this picture. It has been suggested by Bloembergen[19] that optical nonlinearities may be interpreted by adopting an *anharmonic oscillator* model for the material degrees of freedom. This was proposed as a qualitative back of the envelope model. It has been shown[20,21] that molecular assemblies with localized electronic states can indeed be rigorously represented as a collection of anharmonic oscillators representing nonlocal coherences of Frenkel excitons, although the anharmonicity is more complex than a simple cubic nonlinearity.[19]

When applied to molecular assemblies, the sum over

states method shows dramatic cancellations resulting from interferences between single exciton and two exciton transitions.[20–22] These cancellations make it extremely difficult to predict trends since the results are very sensitive to approximations such as truncations. In the oscillator representation, on the other hand, these interferences are naturally built in from the beginning, which greatly facilitates physical intuition. We subsequently extended the oscillator picture to conjugated polyenes with delocalized electronic states. The calculation was based on the Pariser–Pople–Parr (PPP) model for π electrons, which includes both short and long range Coulomb interactions. Many important properties of polyenes can be explained by the model.[23,24,25] By drawing upon the analogy with semiconductors, the Wannier representation (which requires periodic boundary conditions) was used to develop a coupled oscillator picture.[8] The method was shown to reproduce the size scaling and saturation of conjugated polyenes. In this paper we put the oscillator picture on a firmer ground and connect it with more traditional quantum chemistry methods. We calculate the linear and the nonlinear optical response by solving the equations of motion of the single electron reduced density matrix using the time dependent Hartree–Fock (TDHF) approximation.[26] The method can be easily applied to molecules much larger than the exciton coherence length, and can therefore reproduce the size scaling from the small molecules to the bulk (the "thermodynamic limit"). As for the electron correlation problem, since the TDHF approximation describes small amplitude collective quantum fluctuations around the Hartree–Fock ground state, as well as the coupling between these fluctuations, some important correlation effects are taken into account by our method. The TDHF approximation has been used to calculate nonlinear polarizabilities of small molecules.[27] However, it should be particularly applicable for large molecules where the energy surface structure is simpler, and collective motions dominate their optical response.

The density matrix can be expressed using various representations which provide a complementary physical insight. These include the real space, the molecular orbital, and the harmonic oscillator representation. The real space representations allows us to follow directly the charge density and bond order fluctuations induced by the external field. Using these quantities, we can explore the electronic structure of the excitations underlying the optical process. We found that collective CDW like fluctuations and soliton-pair like bond-order fluctuations dominate the linear and the nonlinear optical response of polyacetylene. The molecular orbital representation describes the nonlinear optical process in terms of motions of electrons and holes in the mean field ground state. Finally, the equations of motion of the density matrix can be mapped onto a set of coupled harmonic oscillators. Using this transformation, we can describe the nonlinear optical process in terms of interference among oscillators. This provides an unconventional physical picture which enables us to investigate the mechanism of optical response of various systems (including semiconductors and nonconjugated molecules) from a

unified point of view, and clarifies the connections with other types of materials.

In Sec. II we introduce the PPP Hamiltonian, and a closed equation of motion for the reduced single particle density matrix is derived in Sec. III using the TDHF approximation. In Sec. IV we discuss the real space and the molecular orbital representations of the density matrix, and show how the TDHF equations can be transformed into a set of coupled harmonic oscillators. The first and the third order nonlinear susceptibilities are calculated in Sec. V. Numerical calculations presented in Sec. VI allow us to discuss the nonlinear response functions in terms of charge density and bond order fluctuations. Finally, our results are summarized in Sec. VII.

II. THE PPP HAMILTONIAN

We adopt the PPP Hamiltonian for the π electrons. Many properties of polyenes can be reproduced by this Hamiltonian with the appropriate parameters.[23] We first introduce the following set of binary electron operators:

$$\hat{\rho}_{nm}^{\sigma} = \hat{c}_{m,\sigma}^{\dagger} \hat{c}_{n,\sigma}, \tag{2.1}$$

where $\hat{c}_{n,\sigma}^{\dagger}(\hat{c}_{n,\sigma})$ creates (annihilates) a π electron of spin σ at nth carbon atom. These operators satisfy the Fermi anticommutation relation

$$\{\hat{c}_{m,\sigma}^{\dagger}, \hat{c}_{n,\sigma'}\} = \delta_{m,n}\delta_{\sigma,\sigma'}. \tag{2.2}$$

Using this notation, the PPP Hamiltonian[23] is given by

$$H = H_{\text{SSH}} + H_C + H_{\text{ext}}. \tag{2.3}$$

H_{SSH} is the Su–Schrieffer–Heeger (SSH) Hamiltonian, which consists of the Hückel Hamiltonian with electron–phonon coupling,

$$H_{\text{SSH}} = \sum_{n,m,\sigma} t_{mn}\hat{\rho}_{nm}^{\sigma} + \sum_n \frac{1}{2} K(x_n - \bar{x})^2. \tag{2.4}$$

Here t_{nn} is the Coulomb integral at the nth atom, t_{mn} $(m \neq n)$ is the transfer integral between the nth and mth atoms, K is the harmonic force constant representing the σ-bonds, x_n is the deviation of the nth bond length from the mean bond length along the chain axis z, and $\bar{x}$ is the deviation of the equilibrium σ-bond length (in the absence of π electrons) from that mean. We further assume that an electron can hop only between nearest-neighbor atoms. Thus,

$$t_{nn} = \sum_m \gamma_{nm}, \tag{2.5a}$$

$$t_{nn+1} = t_{n+1n} = \bar{\beta} - \beta' x_n, \tag{2.5b}$$

and $t_{mn} = 0$ otherwise, where γ_{nm} is a repulsion between nth and mth sites. $\bar{\beta}$ is the mean transfer integral and β' is the electron–phonon coupling constant.

H_C represents the electron–electron Coulomb interactions and is given by

$$H_C = \sum_n U\hat{\rho}_{nn}^{\uparrow}\hat{\rho}_{nn}^{\downarrow} + \frac{1}{2}\sum_{n,m,\sigma,\sigma'}^{n \neq m} \gamma_{nm}\hat{\rho}_{nn}^{\sigma}\hat{\rho}_{mm}^{\sigma'}. \tag{2.6}$$

An on-site (Hubbard) repulsion U is given by

$$U = \frac{U_0}{\epsilon}, \tag{2.7}$$

and a repulsion between the nth and the mth sites γ_{nm} is given by the Ohno formula

$$\gamma_{nm} = \frac{U}{\sqrt{1+(r_{nm}/a_0)^2}}, \qquad (2.8)$$

where $U_0 = 11.13$ eV is the unscreened on-site repulsion, ϵ is the dielectric constant which describes the screening by σ-electrons, r_{nm} is the distance between nth and mth sites, and $a_0 = 1.2935$ Å. The parameters are determined so as to reproduce the correct energy gap for polyacetylene (2.0 eV), $\bar{\beta} = -2.4$ eV, $\beta' = -3.5$ eV Å^{-1}, $K = 30$ eV Å^{-2}, $\bar{x} = 0.14$ Å and $\epsilon = 1.5$.

The third term H_{ext} represents the interaction Hamiltonian between the π-electrons and the external electric field $E(t)$. The electric field is assumed to be polarized along the chain axis z. Within the dipole approximation we then have

$$H_{\text{ext}} = -E(t)\hat{P}, \qquad (2.9)$$

where $\hat{P}$ is the molecular polarization operator

$$\hat{P} = -e \sum_{n,\sigma} z(n)\hat{\rho}_{nn}^{\sigma}, \qquad (2.10)$$

where $-e$ is the electron charge and $z(n)$ is the z-coordinate of nth atom.

III. EQUATIONS OF MOTION FOR THE REDUCED DENSITY MATRIX

Starting with the Schrödinger equation, the equation of motion of the expectation value of our binary electron operators

$$\rho_{nm}^{\sigma}(t) = \langle \Psi(t) | \hat{\rho}_{nm}^{\sigma} | \Psi(t) \rangle, \qquad (3.1)$$

is given by

$$i\hbar\dot{\rho}_{nm}^{\sigma}(t) = \langle \Psi(t) | [\hat{\rho}_{nm}^{\sigma}, H] | \Psi(t) \rangle, \qquad (3.2)$$

where $|\Psi(t)\rangle$ is the total many-electron wave function of the system. The expectation values ρ_{nm}^{σ} can be interpreted as elements of the single electron reduced density matrix. Usually the density matrix is defined to have a unit trace. However, this matrix is normalized as

$$\text{Tr } \rho \equiv \sum_{m=1}^{N} \sum_{\sigma} \rho_{mm}^{\sigma} = n_e \qquad (3.3)$$

with N being the total number of sites and n_e is the total number of electrons.

Utilizing the commutation relations (2.2), we can calculate the right-hand side of Eq. (3.2), resulting in

$$i\hbar\dot{\rho}_{nm}^{\sigma}(t) = \sum_i [t_{ni}\rho_{im}^{\sigma}(t) - t_{im}\rho_{ni}^{\sigma}(t)] + U[\langle \hat{\rho}_{nn}^{-\sigma}\hat{\rho}_{nm}^{\sigma} \rangle$$

$$- \langle \hat{\rho}_{mm}^{-\sigma}\hat{\rho}_{nm}^{\sigma} \rangle], + \frac{1}{2} \sum_{i,\sigma'}^{i \neq n} \gamma_{ni}(\langle \hat{\rho}_{ii}^{\sigma'}\hat{\rho}_{nm}^{\sigma} \rangle$$

$$+ \langle \hat{\rho}_{nm}^{\sigma}\hat{\rho}_{ii}^{\sigma'} \rangle) - \frac{1}{2} \sum_{i,\sigma'}^{i \neq m} \gamma_{mi}(\langle \hat{\rho}_{ii}^{\sigma'}\hat{\rho}_{nm}^{\sigma} \rangle$$

$$+ \langle \hat{\rho}_{nm}^{\sigma}\hat{\rho}_{ii}^{\sigma'} \rangle) + e[z(n) - z(m)]E(t)\rho_{nm}^{\sigma}(t), \qquad (3.4)$$

where

$$\langle O \rangle = \langle \Psi(t) | O | \Psi(t) \rangle, \qquad (3.5)$$

and O is an arbitrary operator. These equations of motion are exact, but they are not closed since they contain new higher order variables $\langle \hat{\rho}_{nn}^{-\sigma}\hat{\rho}_{nm}^{\sigma} \rangle$ etc. in the right-hand side. To close the equations, we assume that $|\Psi(t)\rangle$ can be represented by a single Slater determinant at all times (the TDHF approximation).[26] Then the two-electron densities can be factorized into products of single electron densities

$$\langle \hat{\rho}_{nm}^{\sigma}\hat{\rho}_{ij}^{\sigma'} \rangle = \rho_{nm}^{\sigma}(t)\rho_{ij}^{\sigma'}(t) - \delta_{\sigma,\sigma'}\rho_{im}^{\sigma}(t)\rho_{nj}^{\sigma}(t)$$

$$+ \delta_{\sigma,\sigma'}\delta_{n,j}\rho_{im}^{\sigma}(t), \qquad (3.6)$$

and the equations are closed. Substituting Eq. (3.6) into Eq. (3.4), we obtain the TDHF equation

$$i\hbar\dot{\rho}^{\sigma}(t) = [h^{\sigma}(t) + f(t), \rho^{\sigma}(t)], \qquad (3.7)$$

where h^{σ} is the Fock operator matrix corresponding to $H_{\text{SSH}} + H_C$ with spin σ,

$$h_{nm}^{\sigma}(t) = t_{nm} + \delta_{n,m} \sum_{l,\sigma'} \gamma_{nl}\rho_{ll}^{\sigma'}(t) - \gamma_{nm}\rho_{nm}^{\sigma}(t), \qquad (3.8)$$

and $f_{nm}(t)$ is the Fock operator matrix corresponding to H_{ext},

$$f_{nm}(t) = \delta_{n,m}ez(n)E(t). \qquad (3.9)$$

Note that some correlation effects, which are very important in low dimensional systems, are taken into account by the TDHF approximation. In the $f \to 0$ limit, the TDHF coincides with the random phase approximation (RPA) method which describes small amplitude quantum fluctuations around the static mean field solution very well.[26] The solution of the TDHF equation further takes the coupling of the RPA modes into account, as will be shown below.

IV. REAL SPACE, MOLECULAR ORBITAL, AND HARMONIC OSCILLATOR REPRESENTATIONS

We have solved the equations of motion by expanding the single electron density matrix in powers of the external field.[28] The zeroth order solution was taken to be the stationary Hartree–Fock (HF) density matrix, which satisfies

$$[h^{\sigma}, \rho^{\sigma}] = 0. \qquad (4.1)$$

The HF equation was solved numerically by an iterative diagonalization, as shown in Appendix A.

Since both the PPP Hamiltonian and the stationary HF solution are symmetric with respect to spin exchange, the TDHF solution must also have that symmetry. We shall therefore consider the spin symmetric case only, and omit the spin index in the following, denoting

$$\rho = \rho^\uparrow = \rho^\downarrow, \tag{4.2}$$

$$h = h^\uparrow = h^\downarrow. \tag{4.3}$$

We next decompose the density matrix as

$$\rho(t) = \bar{\rho} + \delta\rho(t), \tag{4.4}$$

where $\bar{\rho}$ represents the HF solution. Then the Fock operator matrix is also decomposed in the form

$$h(t) = \bar{h} + \delta h(t), \tag{4.5}$$

where

$$\bar{h}_{nm} = t_{nm} + 2\delta_{n,m}\sum_l \gamma_{nl}\bar{\rho}_{ll} - \gamma_{nm}\bar{\rho}_{nm}, \tag{4.6}$$

$$\delta h_{nm}(t) = 2\delta_{n,m}\sum_l \gamma_{nl}\delta\rho_{ll}(t) - \gamma_{nm}\delta\rho_{nm}(t). \tag{4.7}$$

Substituting the expansions (4.4) and (4.5) into the TDHF Eq. (3.7), we obtain

$$i\hbar\dot{\delta\rho} - [\bar{h},\delta\rho] - [\delta h,\bar{\rho}] = [f,\bar{\rho}] + [f,\delta\rho] + [\delta h,\delta\rho]. \tag{4.8}$$

All terms in the left-hand side are linear in $\delta\rho$. The first two terms in the right-hand side, which are zeroth and first order in $\delta\rho$, respectively, describe the coupling with the radiation field and the last term is quadratic in $\delta\rho$, and comes from Coulomb interaction, as seen from Eq. (4.7).

Hereafter we introduce Liouville space (tetradic) notation for the density matrix. To that end we consider $\delta\rho$ to be an M dimensional vector, rather than an $N\times N$ matrix with N being the number of the atoms and $M=N^2$.[18,29] We thus introduce a new linear vector space, denoted the *Liouville space* in which ordinary operators become M dimensional vectors. The TDHF Eq. (4.8) then assumes the form

$$i\hbar\dot{\delta\rho} - \mathscr{L}\delta\rho = [f,\bar{\rho}] + [f,\delta\rho] + [\delta h,\delta\rho], \tag{4.9}$$

$$\mathscr{L}_{ij,mn}(\omega) = \delta_{j,n}\bar{h}_{im} - \delta_{i,m}\bar{h}_{jn} + 2\delta_{m,n}(\gamma_{in} - \gamma_{jn})\bar{\rho}_{ij}$$
$$- \delta_{i,m}\gamma_{in}\bar{\rho}_{jn} + \delta_{j,n}\gamma_{jm}\bar{\rho}_{im}, \tag{4.10}$$

where $\mathscr{L}$ is an $M\times M$ matrix which is an operator in Liouville space (also denoted superoperator). We shall use script letters to denote Liouville space operators. $\delta\rho$ in the left-hand side is a vector. All terms in the right-hand side $[\delta h,\delta\rho]$ etc. are considered M-dimensional vectors.

So far, all our equations were written using the real space (site) representation. To facilitate the numerical computations and to gain additional physical insight we shall recast the TDHF equation using two additional representations.

We first introduce the Hartree–Fock molecular orbital (HFMO) representation. The transformation of M-dimensional vectors such as $\delta\rho$ from real space to the HFMO representation is defined by

$$\delta\rho_{kk'} = \sum_{mn}\mathscr{V}_{kk',mn}\delta\rho_{mn}, \tag{4.11}$$

where the tetradic transformation matrix $\mathscr{V}$ is

$$\mathscr{V}_{kk',mn} = c_{mk}c_{nk'}, \tag{4.12}$$

and c_{mk} is the normalized HFMO coefficient of the HF orbital k at atom m. As shown in Appendix B, the HFMO representation of $\mathscr{L}$ is given by

$$\tilde{\mathscr{L}} = \mathscr{V}\mathscr{L}\mathscr{V}^T, \tag{4.13}$$

and the TDHF equation in the HFMO representation can be written as

$$i\hbar\dot{\delta\rho} - \tilde{\mathscr{L}}\delta\rho = [f,\bar{\rho}] + [f,\delta\rho] + [\delta h,\delta\rho]. \tag{4.14}$$

Here all the M-dimensional vectors are in the HFMO representation, and we regard $\delta\rho_{kk'}$ as $N\times N$ matrices when we calculate commutators such as $[\delta h,\delta\rho]$. An explicit expression for $\tilde{\mathscr{L}}$ is given in Appendix B. Note that because of the C_{2h} symmetry of the present Hamiltonian, $\tilde{\mathscr{L}}$ is block diagonal into A_g and B_u symmetry parts, which simplifies the numerical calculations.

Our equations can also be mapped onto the equations of motion of coupled harmonic oscillators. This defines a new harmonic oscillator (HO) representation which provides a tremendous physical insight. We analyze the HO representation in the following.

The density matrix $\delta\rho_{kk'}$ defined by Eq. (4.11) is an M-dimensional vector in Liouville space. The number of $\delta\rho_{eh}$ and $\delta\rho_{he}$ components (M_1) is $2n(N-n)$, and the number of $\delta\rho_{ee'}$ and $\delta\rho_{hh'}$ components (M_2) is $(N-n)^2 + n^2$, where $h,h',\ldots$ denote occupied HF orbitals, $e, e',\ldots$ denote unoccupied HF orbitals, and n is the number of the occupied HF orbitals. Since we consider the half-filled and spin symmetric case only, n is half of the number of sites $n=N/2$. We next introduce the Liouville space projection operator P that projects onto the eh and he space. The complementary projection $I-P$ projects onto the ee' and hh' space. We thus have

$$\delta\rho_1 \equiv P\delta\rho = \delta\rho_{eh} + \delta\rho_{he}, \tag{4.15}$$

$$\delta\rho_2 \equiv (I-P)\delta\rho = \delta\rho_{ee'} + \delta\rho_{hh'}, \tag{4.16}$$

where

$$\delta\rho = \delta\rho_1 + \delta\rho_2. \tag{4.17}$$

As shown in Appendix B, the TDHF Eq. (4.8) can be written as

$$i\hbar\dot{\delta\rho}_1 - \tilde{\mathscr{L}}_1\delta\rho_1 = [f,\bar{\rho}] + [f,\delta\rho] + [\delta h_2,\bar{\rho}]$$
$$+ [\delta h,\delta\rho], \tag{4.18}$$

$$i\hbar\dot{\delta\rho}_2 - \hbar\Omega_2\delta\rho_2 = [f,\delta\rho] + [\delta h,\delta\rho], \tag{4.19}$$

where

$$\delta h_{inm}(t) = 2\delta_{n,m}\sum_l \gamma_{nl}\delta\rho_{ill}(t) - \gamma_{nm}\delta\rho_{inm}(t), \tag{4.20}$$

where $i=1,2$. The $M_1\times M_1$ matrix $\tilde{\mathscr{L}}_1$ is the HF stability matrix, and the $M_2\times M_2$ matrix Ω_2 is diagonal in Liouville space and its diagonal matrix elements are given by the

difference of the HF eigenvalues. Thus, if $\Omega_{2\nu}$ is a diagonal element then $-\Omega_{2\nu}$ is an eigenvalue as well. Their explicit expressions are given in Appendix B. The matrix $\mathscr{L}_1$ can be diagonalized by the $M_1 \times M_1$ matrix w as

$$w\mathscr{L}_1 w^{-1} = \hbar\Omega_1, \qquad (4.21)$$

where Ω_1 is an $M_1 \times M_1$ diagonal matrix. The $M_1/2$ diagonal elements of Ω_1 are RPA energies $\Omega_{1\nu} > 0$ and the other $M_1/2$ diagonal elements are $\Omega_{\bar{\nu}} = -\Omega_\nu$.[26] We obtain w numerically as described in Appendix B. Then, the transformation of Liouville space vectors such as $\delta\rho$ from real space to the HO representation is defined by

$$\delta\rho_\nu = \sum_{mn} \mathscr{U}_{\nu,mn}\delta\rho_{mn}. \qquad (4.22)$$

The transformation matrix $\mathscr{U}$ is given by

$$\mathscr{U} = \mathscr{W}\mathscr{V}, \qquad (4.23)$$

and the $M \times M$ matrix $\mathscr{W}$ is given by

$$\mathscr{W} = \begin{bmatrix} w & 0 \\ 0 & I \end{bmatrix}, \qquad (4.24)$$

where we arrange the M-components of the vectors in Liouville space in the following manner: we put the interband $\delta\rho_{eh}$ and $\delta\rho_{eh}$ components ($\delta\rho_1$) in the first M_1 rows, and the intraband $\delta\rho_{ee'}$ and $\delta\rho_{hh'}$ components ($\delta\rho_2$) in the remaining M_2 rows, namely,

$$\delta\rho = \begin{pmatrix} \delta\rho_{eh} \\ \delta\rho_{he} \\ \delta\rho_{ee} \\ \delta\rho_{hh} \end{pmatrix}. \qquad (4.25)$$

It is shown in Appendix B, that the TDHF equation can be recast in the HO representation as

$$i\hbar\dot{\delta\rho}_\nu - \hbar\Omega_\nu\delta\rho_\nu = F_\nu + \sum_{\nu'} G_{\nu,\nu'}\delta\rho_{\nu'} + \sum_{\nu'}^{\nu' \subset M_2} R_{\nu,\nu'}\delta\rho_{\nu'}$$

$$+ \sum_{\nu'\nu''} S_{\nu,\nu'\nu''}\delta\rho_{\nu'}\delta\rho_{\nu''}, \qquad (4.26)$$

where Ω_ν is the diagonal element of Ω_1 or Ω_2, the summation in the third term of the right-hand side is done over the M_2 components, and explicit expressions for F, G, R, and S are given in Appendix B.

The physical significance of the right-hand side of Eq. (4.26) is as follows. The first term corresponds to the first term of the right-hand side of Eq. (4.18) and represents the driving force due to the external field. The second term corresponds to the second and the first terms of the right-hand side of Eqs. (4.18) and (4.19), respectively, and describes the interaction between the external field and $\delta\rho$. Thus the F and the G terms are induced by the external field. The third term corresponds to the third term of the right-hand side of Eq. (4.18) and describes the coupling of $\delta\rho_1$ and $\delta\rho_2$. The nonlinear fourth term corresponds to the fourth and the second terms of the right-hand side of Eqs. (4.18) and (4.19), respectively, and represents anhar-

monic coupling among the oscillators. As seen from Eqs. (4.7) and (4.20), these R and S terms containing δh are induced by the Coulomb interaction.

To demonstrate the physical significance of this transformation, let us temporarily neglect the right-hand side of this equation. Then the TDHF equation assumes the form

$$i\dot{\delta\rho}_\nu - \Omega_\nu\delta\rho_\nu = 0. \qquad (4.27)$$

As shown before, both in Ω_1 and Ω_2, the diagonal elements always come in pairs; if Ω_ν is an eigenvalue then $-\Omega_\nu$ is an eigenvalue as well. We shall denote the corresponding eigenvectors $\delta\rho_\nu$ and $\delta\rho_{\bar{\nu}}$, respectively. By introducing new variables, a coordinate

$$Q_\nu \equiv \delta\rho_\nu + \delta\rho_{\bar{\nu}}, \qquad (4.28)$$

and a momentum

$$P_\nu \equiv -i\Omega_\nu(\delta\rho_\nu - \delta\rho_{\bar{\nu}}), \qquad (4.29)$$

we can rewrite these linearized equations of motion as

$$\dot{Q}_\nu = P_\nu, \qquad (4.30)$$

$$\dot{P}_\nu = -\Omega_\nu^2 Q_\nu. \qquad (4.31)$$

This pair of equations represent a harmonic oscillator with frequency Ω_ν. We have thus mapped Eq. (4.9) onto the equations of motions of $M/2$ coupled harmonic oscillators (4.26).

A HO representation could be most naturally defined by using the normal modes of the entire linear term [left-hand side of Eq. (4.9)], the transformation matrix $\mathscr{U}$ could then be defined by the following relation:

$$\mathscr{U}\mathscr{L}\mathscr{U}^{-1} = \hbar\Omega, \qquad (4.32)$$

where $\hbar\Omega$ is a diagonal matrix whose elements are the eigenvalues of $\mathscr{L}$. The reasons why we do not define the normal modes of $\mathscr{L}$ as oscillators are as follows. First, the present oscillators defined by our method consist of $M_1/2$ oscillators which are RPA normal modes and $M_2/2$ oscillators which are single electron–electron or hole–hole pairs as shown in Appendix B. Thus, the oscillators have a clear physical meaning. Second, we need to diagonalize an $M_1 \times M_1$ matrix to obtain oscillators in our method [see Eq. (4.21)], whereas we need to diagonalize the full $M \times M$ matrix to obtain oscillators defined by Eq. (4.32). Thus the present oscillators are more convenient for practical numerical calculations. Furthermore, the $M_1/2$ oscillators, which come from $\delta\rho_1$, have a collective nature,[22] whereas the $M_2/2$ oscillators, which come from $\delta\rho_2$, simply represent single electron–electron or hole–hole pair. Thus, the coupling between $M_1/2$ and $M_2/2$ oscillators, namely, the R term is weak. This suggests that the difference between the present oscillators and the more rigorous set defined by Eq. (4.32) is small.

Since $\mathscr{L}_1$ is block diagonal into A_g and B_u symmetry parts, all the oscillators, which diagonalize $\mathscr{L}_1$, may be classified into either A_g or B_u symmetries. As seen from Eq. (B25), $S_{\nu,\nu'\nu''} \neq 0$ when, for example, ν is an A_g (B_u) oscillator and ν' and ν'' are B_u and B_u(B_u and A_g) oscillators. This indicates that A_g and B_u oscillators do couple in the equation of motion. This is in contrast to the descrip-

tion in terms of the eigenstates of the Hamiltonian, where A_g and B_u states do not couple at all. This fundamental difference between the oscillator and the eigenstate expansions is related to the nonlinear form of the present equation, as opposed to eigenstate expansions which are linear (a product of an A_g and a B_u variables can have a B_u character). Potentially this allows for a relatively inexpensive way of describing complex physical situations, compared with eigenstate expansions.

V. NONLINEAR OPTICAL POLARIZABILITIES

To compute the nonlinear optical polarizabilities, we expand $\delta\rho$ in powers of the external field

$$\delta\rho(t) = \rho^{(1)}(t) + \rho^{(2)}(t) + \rho^{(3)}(t) + \cdots, \tag{5.1}$$

where $\rho^{(q)}(t)$ is the qth order density matrix of the TDHF solution. The Fock operator matrix is further expanded in powers of the external field as

$$\delta h(t) = h^{(1)}(t) + h^{(2)}(t) + h^{(3)}(t) + \cdots, \tag{5.2}$$

where

$$h_{nm}^{(q)}(t) = 2\delta_{n,m} \sum_l \gamma_{nl}\rho_{ll}^{(q)}(t) - \gamma_{nm}\rho_{nm}^{(q)}(t). \tag{5.3}$$

Substituting Eqs. (5.1) and (5.2) into Eqs. (4.9), we obtain the first, the second, and the third order equations of motions,

$$i\hbar\dot{\rho}^{(1)}(t) - \mathscr{L}\rho^{(1)}(t) = [f(t),\bar{\rho}], \tag{5.4a}$$

$$i\hbar\dot{\rho}^{(2)}(t) - \mathscr{L}\rho^{(2)}(t) = [h^{(1)}(t),\rho^{(1)}(t)]$$
$$+ [f(t),\rho^{(1)}(t)], \tag{5.4b}$$

$$i\hbar\dot{\rho}^{(3)}(t) - \mathscr{L}\rho^{(3)}(t) = [h^{(1)}(t),\rho^{(2)}(t)]$$
$$+ [h^{(2)}(t),\rho^{(1)}(t)]$$
$$+ [f(t),\rho^{(2)}(t)]. \tag{5.4c}$$

Taking the Fourier transform of Eqs. (5.4) defined by

$$g(\omega) \equiv \frac{1}{\sqrt{2\pi}} \int_{-\infty}^{+\infty} g(t)\exp(i\omega t)dt, \tag{5.5}$$

where $g(t)$ is an arbitrary function of t, we obtain the equations of motions in the frequency-domain,

$$\hbar\omega\rho^{(1)}(\omega) - \mathscr{L}\rho^{(1)}(\omega) = [f(\omega),\bar{\rho}], \tag{5.6a}$$

$$\hbar\omega\rho^{(2)}(\omega) - \mathscr{L}\rho^{(2)}(\omega)$$
$$= \frac{1}{\sqrt{2\pi}} \int_{-\infty}^{\infty} \{[h^{(1)}(\omega'),\rho^{(1)}(\omega-\omega')]$$
$$+ [f(\omega'),\rho^{(1)}(\omega-\omega')]\}d\omega', \tag{5.6b}$$

$$\hbar\omega\rho^{(3)}(\omega) - \mathscr{L}\rho^{(3)}(\omega)$$
$$= \frac{1}{\sqrt{2\pi}} \int_{-\infty}^{\infty} \{[h^{(1)}(\omega'),\rho^{(2)}(\omega-\omega')]$$
$$+ [h^{(2)}(\omega'),\rho^{(1)}(\omega-\omega')]$$
$$+ [f(\omega'),\rho^{(2)}(\omega-\omega')]\}d\omega'. \tag{5.6c}$$

Next, we define a new tetradic $(M \times M)$ Green function $\mathscr{G}(\omega)$ by the following equation:

$$\mathscr{G}_{ij,mn}^{-1}(\omega) = \hbar\omega\delta_{i,m}\delta_{j,n} - \mathscr{L}_{ij,mn}(\omega). \tag{5.7}$$

From Eqs. (5.6) and inverting the matrix, we obtain

$$\rho^{(1)}(\omega) = \mathscr{G}(\omega)[f(\omega),\bar{\rho}], \tag{5.8a}$$

$$\rho^{(2)}(\omega) = \mathscr{G}(\omega)\frac{1}{\sqrt{2\pi}} \int_{-\infty}^{+\infty} \{[h^{(1)}(\omega'),\rho^{(1)}(\omega-\omega')]$$
$$+ [f(\omega'),\rho^{(1)}(\omega-\omega')]\}d\omega', \tag{5.8b}$$

$$\rho^{(3)}(\omega) = \mathscr{G}(\omega)\frac{1}{\sqrt{2\pi}} \int_{-\infty}^{+\infty} \{[h^{(1)}(\omega'),\rho^{(2)}(\omega-\omega')]$$
$$+ [h^{(2)}(\omega'),\rho^{(1)}(\omega-\omega')]$$
$$+ [f(\omega'),\rho^{(2)}(\omega-\omega')]\}d\omega'. \tag{5.8c}$$

In this way, we can obtain iteratively the TDHF solution to arbitrary order in the external field. To reduce computational time, we have adopted a somewhat different route for solving these equations. The method is outlined in Appendix C. However, the difference is purely technical and the method is equivalent to the real space representation described here. We have added a damping term to the TDHF equation as described in Appendix C. This damping provides a finite linewidth to the optical resonances and can represent a simple line broadening mechanism (e.g., due to coupling with phonons) or a finite spectral resolution.

The expectation value of the total polarization operator of a single molecule

$$P(t) \equiv \langle \Psi(t)|\hat{P}|\Psi(t)\rangle,$$

is

$$P(t) = -2e \sum_n z(n)\rho_{nn}(t). \tag{5.9}$$

We shall expand $P(t)$ in powers of the external field

$$P(t) = P^{(1)}(t) + P^{(2)}(t) + P^{(3)}(t) + \cdots, \tag{5.10}$$

where $P^{(q)}(t)$ is the total polarization to qth order and $P^{(0)}(t) = 0$. From Eqs. (5.1) and (5.9), we see that $P^{(q)}(t)$ is given by

$$P^{(q)}(t) = -2e \sum_n z(n)\rho_{nn}^{(q)}(t), \tag{5.11}$$

where $\rho_{nn}^{(q)}(t)$ is obtained by taking the inverse Fourier transform of $\rho_{nn}^{(q)}(\omega)$. Using $P^{(q)}(t)$ and $\rho^{(q)}(\omega)$, we obtain our final expressions for the optical polarizabilities (see Appendix D),

$$\alpha(-\omega;\omega) = -\frac{1}{E_1}\frac{4e}{\sqrt{2\pi}} \sum_n z(n) \tilde{\rho}_{nn}^{(1)}(-\omega;\omega), \tag{5.12}$$

$$\gamma(-3\omega;\omega,\omega,\omega) = -\frac{1}{E_1^3}\frac{4e}{\sqrt{2\pi}} \sum_n z(n) \tilde{\rho}_{nn}^{(3)}(-3\omega;\omega,\omega,\omega). \tag{5.13}$$

Equation (5.13) gives the third order polarizability that is responsible for THG. Other four wave mixing processes can simply be described by changing the frequency arguments. Extension to higher nonlinearities is also straightforward.

VI. NUMERICAL RESULTS

In this section, we apply our method to the half-filled PPP model for polyacetylene with $N=60$. In all calculations we used the PPP parameters given in Sec. II. The damping rate [see Eqs. (C10)] was taken to be $\Gamma=0.1$ eV. We shall follow the dynamics of two important physical quantities which are affected by the coupling to the radiation field. First, the charge density at the nth atom, which determines the total polarization is defined by

$$d_n \equiv 1 - 2\rho_{nn}. \tag{6.1}$$

The second quantity is the bond order of the nth bond (p_n) which is closely related to the stabilization mechanism of the HF ground state, and is defined by

$$p_n \equiv \rho_{nn+1} + \rho_{n+1n}. \tag{6.2}$$

We further introduce the bond order parameter, which measures the strength of bond order alternation

$$p_n' \equiv (-1)^{n-1}(p_n - \bar{p}), \tag{6.3}$$

where $\bar{p}$ is the average bond order. It is obtained from Eq. (A7) as

$$\bar{p} = -\frac{K\bar{x}}{2\beta'}. \tag{6.4}$$

The geometry optimized HF ground state of the present Hamiltonian is a bond order wave (BOW), where p_n alternates between every two bonds and $d_n=0$. The HF ground state has an almost uniform bond order parameter $(p_n' = 0.24)$, as shown in Fig. 1. Note that because of boundary effects, the bond order parameter increases near the chain edge. As seen from Eq. (A7), the bond order parameter is proportional to the strength of bond length alternation, which gives the alternation of tranfer integral as seen from Eq. (2.5). Thus, the transfer integral β_n can be approximated by $\beta_n = \bar{\beta}[1 - (-1)^n \delta]$ where $\delta = 0.082$ in this case except for the chain edge region. The BOW structure is stabilized by the exchange, the Coulomb, and the electron–phonon interactions.[21]

As indicated earlier, the TDHF equation is mapped onto the equations of motion of $M/2$ coupled harmonic
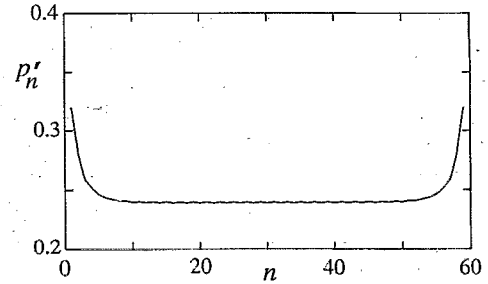

FIG. 1. The bond order parameter distribution of the Hartree–Fock ground state.

oscillators. These include $M_1/2$ oscillators which correspond to the eigenvalues of Ω_1 and $M_2/2$ oscillators which correspond to the eigenvalues of Ω_2. These oscillators have very different physical properties. Since the $M_1/2$ oscillators are the normal modes of the RPA equation, they have a collective nature, that is, they are formed by coherent superpositions of many electron-hole pairs. This collective property strongly affects the optical response as shown in the following.

As far as the linear response is concerned, the system behaves as a collection of harmonic oscillators (the anharmonicities only affect the nonlinear response). Consequently, the linear optical susceptibility $\alpha(-\omega;\omega)$ can be recast in the Drude form (see Appendix C),

$$\alpha(-\omega;\omega) = \frac{e^2}{m} \sum_\nu \frac{f_\nu}{(\omega+i\Gamma)^2 - \Omega_{1\nu}^2}, \tag{6.5}$$

where the summation is performed over the $M_1/2$ oscillators, the oscillator strength f_ν of the νth oscillator is given by

$$f_\nu = \frac{4m\Omega_{1\nu}}{\hbar}\left[\sum_{eh} z_{eh}(X_{eh,\nu} + Y_{eh,\nu})\right]^2, \tag{6.6}$$

and m has the unit of mass and determined to give $\Sigma_\nu f_\nu = N$, m is 1.66 m_e and 1.59 m_e in the PPP and SSH models, respectively, where m_e is the mass of an electron.

From Eq. (6.6), we see that the collective harmonic oscillators have a large oscillator strength coming from the sum of contributions of the various electron and hole states. The extremely large oscillator strength of the lowest frequency $M_1/2$ oscillators as shown in Fig. 2 reflects their collective nature. These oscillators, therefore, dominate the linear optical response function. On the other hand, each of the remaining $M_2/2$ oscillators can be regarded as representing a single electron–electron or hole–hole pair. Consequently, their oscillator strengths vanish [see Eq. (4.19)], and they couple very weakly with the optically active collective oscillators. Thus they play only a secondary role in the optical response. Hereafter, we consider only the $M_1/2$ oscillators and refer to them simply as the oscillators.

The oscillators can be further classified into A_g and B_u type. The oscillator strength of the A_g oscillators vanishes.
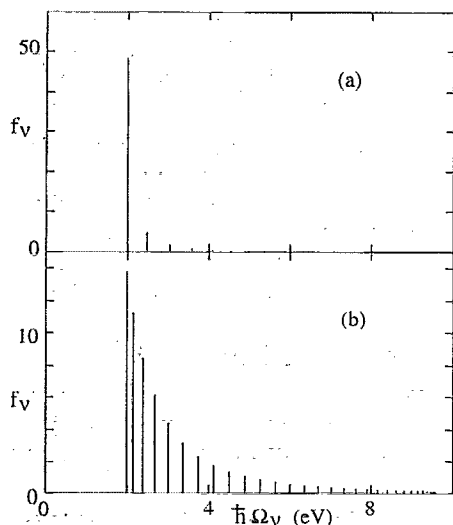
FIG. 2. The oscillator strength of the B_u oscillators is plotted vs their frequencies in the PPP and Hückel models.

Nevertheless, since collective A_g oscillators strongly couple with collective B_u oscillators, they do affect the nonlinear optical processes and cannot be neglected.

We first discuss the electronic structure of the collective oscillators. To that end we return to the linearized form of TDHF Eq. (B3) in the absence of the field where we set the right-hand side to zero. We shall look for eigenmodes of this equation by assuming a solution of the form

$$\delta\rho(t) = \delta\rho(\nu)\exp(-i\Omega_\nu t). \tag{6.7}$$

We then obtain the eigenvalue problem

$$[\bar{h},\delta\rho(\nu)] + [\delta h,\bar{\rho}] = \hbar\Omega_\nu\rho(\nu). \tag{6.8}$$

This equation can be solved using the transformation matrix $\mathcal{U}$, and the eigenvectors in the real space representation are given by

$$\delta\rho(\nu)_{mn} = \mathcal{U}^{-1}_{mn,\nu}. \tag{6.9}$$

The charge density induced by the νth oscillator is given by

$$\delta d(\nu)_n = \delta\tilde{d}(\nu)_n \exp(i\Omega_\nu t), \tag{6.10}$$

and the corresponding bond order is

$$\delta p(\nu)_n = \delta\tilde{p}(\nu)_n \exp(i\Omega_\nu t). \tag{6.11}$$

Here

$$\delta\tilde{d}(\nu)_n = -2\mathcal{U}^{-1}_{nn,\nu}, \tag{6.12}$$

$$\delta\tilde{p}(\nu)_n = \mathcal{U}^{-1}_{nn+1,\nu} + \mathcal{U}^{-1}_{n+1n,\nu}. \tag{6.13}$$

We show the amplitudes of the oscillating charge density $\delta\tilde{d}_n$ and the bond order parameter $\tilde{p}'_n = (-1)^{n-1}\delta\tilde{p}_n$ of the six lowest frequency A_g and B_u oscillators in Fig. 3, where we label the oscillators in order of increasing frequency by $A_g(\nu)$ and $B_u(\nu)$, $\nu=1,2,...$. Since either the charge density or the bond order of each oscillator is zero, we show only the nonvanishing quantity in each case. Note that only B_u oscillators with charge density have a nonzero os-
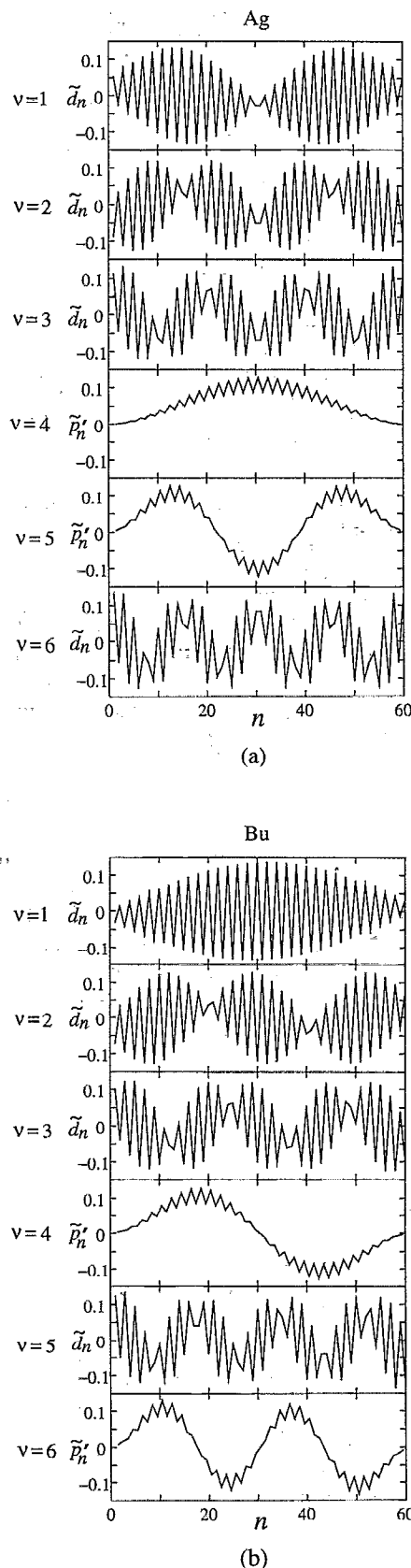

(a)

(b)

FIG. 3. The charge density or bond order parameter oscillation amplitude of the lowest frequency harmonic oscillators. Since either the charge density or the bond order parameter fluctuations vanishes for each oscillator, we show only the nonzero parameter in each case. (a) A_g oscillators and (b) B_u oscillators.

TABLE I. The frequency (Ω_v), oscillator strength (fv), charge density (d_n), and bond order (p_n) of the 12 lowest frequency oscillators.

Oscillator	$\hbar\Omega_v$ (eV)	fv	d_n	p_n
$B_u(1)$	1.99	48.3	0	X
$A_g(1)$	2.21	0	0	X
$B_u(2)$	2.47	4.84	0	X
$A_g(2)$	2.75	0	0	X
$B_u(3)$	3.03	1.78	0	X
$A_g(3)$	3.31	0	0	X
$A_g(4)$	3.38	0	X	0
$B_u(4)$	3.46	0	X	0
$B_u(5)$	3.57	0.93	0	X
$A_g(5)$	3.58	0	X	0
$B_u(6)$	3.73	0	X	0
$A_g(6)$	3.83	0	0	X

cillator strength. The $B_u(1)$, $A_g(1)$, $B_u(2)$, $A_g(2)$, $B_u(3)$, $A_g(3)$, $B_u(5)$, and $A_g(6)$ oscillators (in order of increasing frequency) have a CDW like electronic structures and have 0, 1, 2,..., 7 nodes, respectively. The CDW is stabilized by the Madelung energy and is very stable particularly in one-dimensional systems.[21] The $A_g(4)$, $B_u(4)$, $A_g(5)$, and $B_u(6)$ oscillators (in order of increasing frequency) have an oscillating bond order parameter, and have 0, 1, 2,..., 3 nodes, respectively. Since the bond order parameter, which shows the strength of bond order alternation, is locally increased or decreased, they have a soliton pair like electronic structure.[23] The properties of the 12 lowest frequency oscillators are summarized in Table I.

In Fig. 4, we display the linear absorption $\{\text{Im}[\alpha(-\omega;\omega)]\}$ and the absolute value of the third order polarizability connected to THG ($|\gamma(-3\omega;\omega,\omega,\omega)|$). We label the resonances in these spectra by A, B,..., E and a, b,..., g, respectively as indicated in the figure. In order to compare the three-photon resonances with the linear absorption, we have plotted $|\gamma|$ vs $3\hbar\omega$. The $\hbar\omega$ dependence

of $|\gamma|$ for polyacetylene was measured in the frequency range of 0.4 eV $< \hbar\omega < 1.2$ eV.[30,31] A strong peak is observed at 0.5–0.6 eV, and a much weaker peak is observed at 0.8 eV. The former and the latter correspond to the peaks a and b, respectively, in our calculation. Our result is consistent with experiment, except that the tail of peak c is not observed in the experiment. This may indicate that we have either overestimated the strength of peak c, or that the damping constant used here is too large for the peak c (we have used the same damping constant for all oscillators).

To investigate the mechanism and the electronic dynamics underlying the nonlinear optical response, we next examine the electronic structure induced by the external electric field. Taking the inverse Fourier transformation of Eqs. (D5), (D7), and (D10), and then using Eq. (D13), we obtain the single electron density matrices induce by the external field $E(t) = E_1 \cos\omega_1 t$ order by order in the field

$$\rho^{(1)}(t) = \frac{1}{\sqrt{2\pi}}\{\text{Re}[\tilde{\rho}^{(1)}(-\omega_1;\omega_1)]\cos(\omega_1 t)$$
$$+ \text{Im}[\tilde{\rho}^{(1)}(-\omega_1;\omega_1)]\sin(\omega_1 t)\}, \quad (6.14a)$$

$$\rho^{(2)}(t) = \frac{1}{\sqrt{2\pi}}\{\text{Re}[\tilde{\rho}^{(2)}(-2\omega_1;\omega_1,\omega_1)]\cos(2\omega_1 t)$$
$$+ \text{Im}[\tilde{\rho}^{(2)}(-2\omega_1;\omega_1,\omega_1)]\sin(2\omega_1 t) + \cdots\}, \quad (6.14b)$$

$$\rho^{(3)}(t) = \frac{1}{\sqrt{2\pi}}\{\text{Re}[\tilde{\rho}^{(3)}(-3\omega_1;\omega_1,\omega_1,\omega_1)]\cos(3\omega_1 t)$$
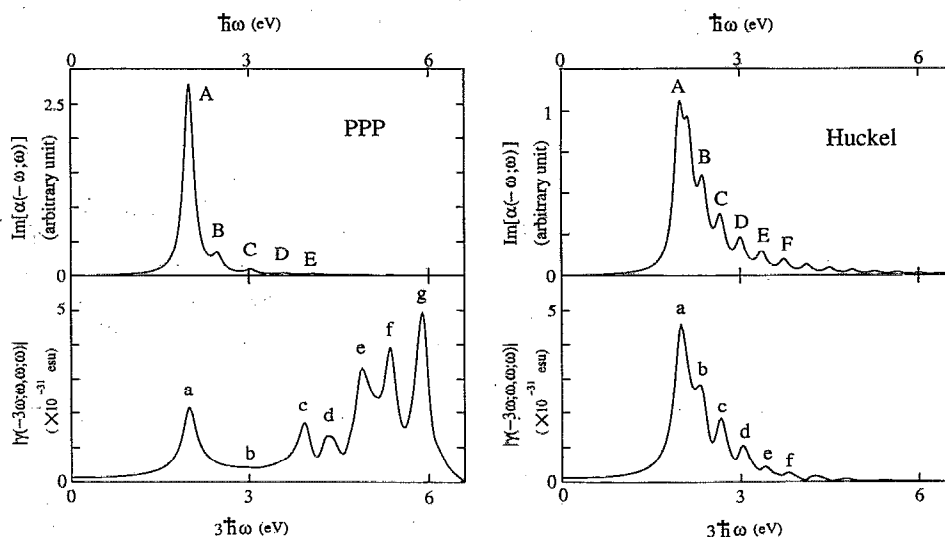$$+ \text{Im}[\tilde{\rho}^{(3)}(-3\omega_1;\omega_1,\omega_1,\omega_1)]\sin(3\omega_1 t) + \cdots\}. \quad (6.14c)$$

FIG. 4. The linear absorption spectrum $\text{Im}[\alpha(-\omega;\omega)]$ is plotted vs the frequency ω, and compared with the absolute value of the hyperpolarizability $|\gamma(-3\omega;\omega,\omega,\omega)|$ connected to THG which is plotted vs 3ω. Left column, PPP model; right column, Hubbel model.
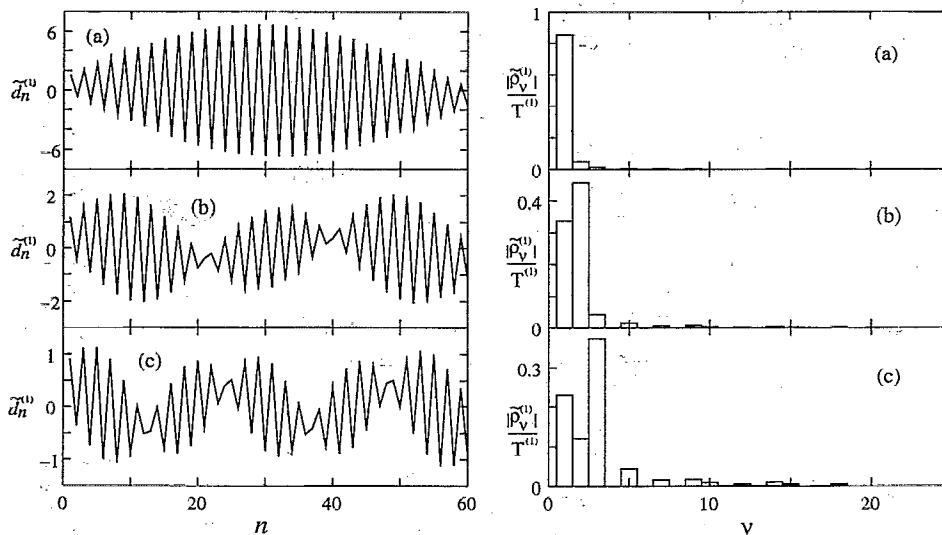
FIG. 5. Left column, the first order amplitude of the charge density oscillation induced by the external field at the frequencies of the absorption peaks $\hbar\omega=$ (a) 1.99; (b) 2.46; and (c) 3.03 eV. We show only the amplitudes $\mathrm{Im}[\tilde{\rho}_{nn}^{(1)}(\omega)]$ oscillating out of phase with the external field. Right column, the normalized absolute value of the corresponding first order density matrix in the harmonic oscillator representation, where $\tilde{\rho}_{\nu}^{(1)}(\omega)$ is the component of the first order density matrix corresponding to the $B_u(\nu)$ oscillator and the normalization constant is $T^{(1)}=\sum_{\nu}|\tilde{\rho}_{\nu}^{(1)}|$. The applied external electric field is 10^8 V/m.

Note that these equations hold regardless of the representation (whether the real space, HFMO or HO). As seen from Eqs. (D8a) and (D11a), these quantities can be calculated successively; $\gamma(-3\omega_1;\omega_1,\omega_1,\omega_1)$ is obtained only from $\tilde{\rho}^{(3)}(-3\omega_1;\omega_1,\omega_1,\omega_1)$, which in turn is obtained from $\tilde{\rho}^{(2)}(-2\omega_1;\omega_1,\omega_1)$ and $\tilde{\rho}^{(1)}(-\omega_1;\omega_1)$, and $\tilde{\rho}^{(2)}(-2\omega_1;\omega_1,\omega_1)$ is obtained from $\tilde{\rho}^{(1)}(-\omega_1;\omega_1)$. We have kept only terms which contribute to $\gamma(-3\omega_1;\omega_1,\omega_1,\omega_1)$, and all other terms were omitted in these expressions. The single electron density matrices have a term oscillating in phase with the external electric field and a term oscillating out of the phase. The amplitudes of the former terms are given by $\mathrm{Re}[\tilde{\rho}^{(q)}]$ and they contribute to the real parts of the linear and nonlinear polarizabilities, and those of the latter terms are given by $\mathrm{Im}[\tilde{\rho}^{(q)}]$ and they contribute to the imaginary parts. Since the charge density is related to the diagonal elements of the density matrix in the real space representation, it also has terms oscillating in phase and out of the phase with the external electric field,

$$d_n^{(q)}(t)=\frac{1}{\sqrt{2\pi}}\{\mathrm{Re}[\tilde{d}_n^{(q)}(q\omega_1)]\cos(2\omega_1 t)$$
$$+\mathrm{Im}[\tilde{d}_n^{(q)}(q\omega_1)]\sin(2\omega_1 t)+\cdots\}, \quad (6.15)$$

and

$$\tilde{d}_n^{(q)}(q\omega_1)=-2\tilde{\rho}_{nn}^{(q)}(-q\omega_1;\ldots). \quad (6.16)$$

The bond order induced by the external field also has both types of terms, and the amplitude is given by

$$\tilde{p}_n^{(q)}(q\omega_1)=\tilde{\rho}_{nn+1}^{(q)}(-q\omega_1;\ldots)+\tilde{\rho}_{n+1n}^{(q)}(-q\omega_1;\ldots). \quad (6.17)$$

To analyze the charge dynamics underlying the absorption spectra, we investigate the first order charge density induced by the external field. In Fig. 5 we show $\mathrm{Im}[\tilde{d}_n^{(1)}]$ at the frequencies of the absorption peaks A, B, and C. We show only the imaginary parts because they are strongly enhanced at the resonance frequencies. However, the charge density distributions of the real and the imaginary parts are quite similar at every frequency. At the frequencies of the peaks A, B, and C, the induced charge distributions have CDW like structures which are quite similar to those of oscillators $B_u(1)$, $B_u(2)$, and $B_u(3)$, respectively. To see this more directly, we display in Fig. 5 the absolute value of the components of the density matrix in the HO representation, where $|\delta\rho_{\nu}^{(1)}|$ shows the component corresponding to the $B_u(\nu)$ oscillator. At the frequency of peak A, the component corresponding to $B_u(1)$ is much larger than the other components. Thus, peak A can be assigned to the $B_u(1)$ oscillator. At the frequency of peaks B and C, the components corresponding to $B_u(2)$ and $B_u(3)$ are the largest, respectively, but the $B_u(1)$ oscillator also has a large contribution at both frequencies. Thus, peaks B and C can be assigned to the $B_u(2)$ and $B_u(3)$ oscillators, respectively, although the contribution from the off-resonant $B_u(1)$ oscillator is still large because of its huge oscillator strength. At these most prominent peaks, the components of the three lowest energy B_u oscillators are much larger than the other components. Therefore, we conclude that the absorption spectrum is dominated by the characteristic CDW like charge density fluctuations of these collective $B_u(1)$, $B_u(2)$, and $B_u(3)$ oscillators. Since these peaks in absorption are below the HF energy gap, these charge density fluctuations can be regarded as excitons. However, these excitons are not simple electron–hole pairs but have the characteristic collective nature of electronic structure of one-dimensional systems.
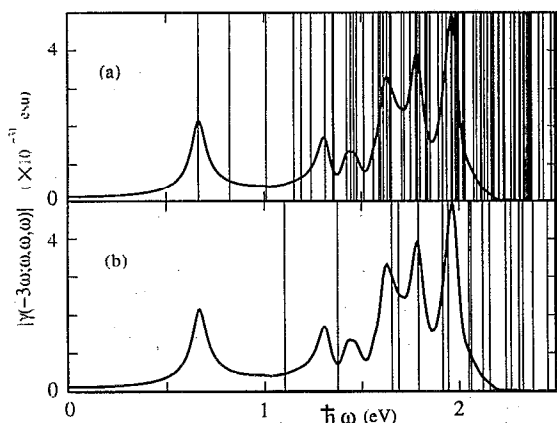
FIG. 6. The THG hyperpolarizability $|\gamma(-3\omega;\omega,\omega,\omega)|$ is plotted vs ω. (a) One-third of the frequencies of the B_u harmonic oscillators and (b) half the frequencies of the A_g harmonic oscillators are also shown in order to highlight three photon and two photon resonances respectively.

We next consider the frequency dispersion of $|\gamma(-3\omega;\omega,\omega,\omega)|$. To compare the frequencies of the peaks and the oscillators, we display in Fig. 6 the frequency dependence of $|\gamma|$, one-third the frequencies of B_u oscillators, and half the frequencies of A_g oscillators. There are some near resonant oscillators at each peak as seen from Fig. 6. However, this comparison is not sufficient to identify the origins of the peaks. As will be shown later, we need to examine the density matrix in each order for such identification. This further provides important physical insight. In Figs. 7, 8, and 9 we show the density matrices to first, second, and third order in the external field, using the real space and the HO representations. In the real space representation, we show only $\tilde{d}_n^{(q)}(q\omega_1)$ in the first and

third order and $\tilde{p}_n'^{(q)}(q\omega_1) \equiv (-1)^n \tilde{p}_n^{(q)}(q\omega_1)$ in the second order because bond order is zero in the first and third orders and charge density is zero in the second order. Similarly, in the HO representation, we show only the B_u oscillator components in the first and third orders and only the A_g oscillator components in the second order, since all other components vanish. These properties follow directly from the symmetry of our Hamiltonian.

We focused on the following frequencies $\hbar\omega = 1.97$ eV corresponding the peak A in absorption and the peak g in THG (Fig. 7), $\hbar\omega = 1.63$ eV corresponding the peak e in THG (Fig. 8), and $\hbar\omega = 0.67$ eV corresponding the peak a in THG (Fig. 9). We first consider the density matrices at $\hbar\omega = 1.97$ eV. The frequency of the $B_u(1)$ oscillator is resonant with this frequency, so that the component corresponding to this oscillator is much larger than the other components in the first order. Moreover, the amplitude of charge density oscillation is much larger than the other two frequencies. In the second order, half the frequency of $A_g(7)$ is the closest to 1.97 eV. However, the component corresponding to the oscillator is not large but that corresponding to $A_g(4)$ is the largest, and we can observe the characteristic soliton pair like bond order oscillation pattern of this oscillator in the real space representation. Only B_u oscillators with charge density contribute to the first order density matrix. Moreover, only $A_g(\nu)$ oscillators with bond order ($\nu = 4,5,7,...$) contribute to the second order density matrix because A_g oscillators with charge density do not couple with B_u oscillators with charge density. For the same reason, only B_u oscillators with charge density contribute to the third order density matrix. Since $A_g(4)$ strongly couples with $B_u(1)$, which dominates the first order density matrix, the $A_g(4)$ oscillator is strongly excited although it is off resonant at that frequency. There
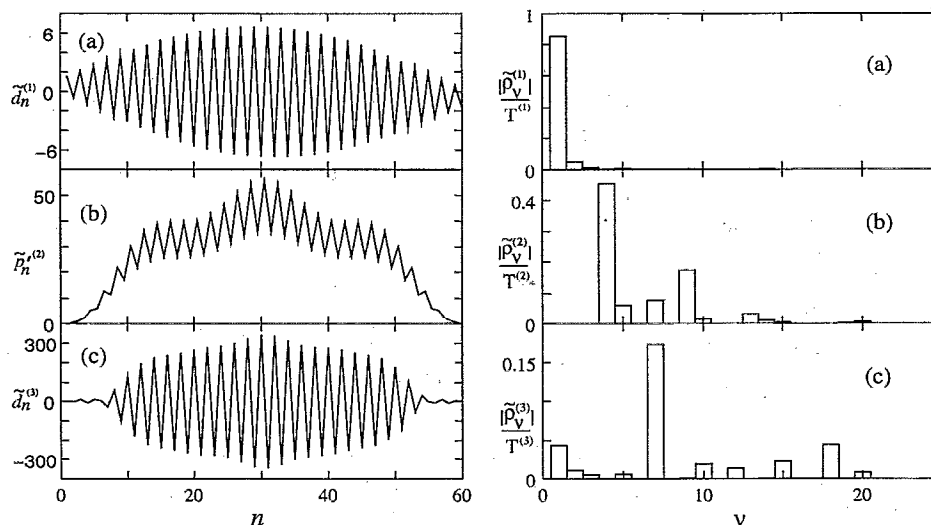

FIG. 7. Left column (a) the first order amplitude of charge density oscillation; (b) second order amplitude of bond order parameter oscillation; and (c) the third order amplitude of charge density oscillation induced by the external field. Right column, the normalized absolute values of the same order density matrices in the harmonic oscillator representation. $\tilde{p}_\nu^{(q)}(q\omega)$ is the component of the qth order density matrix corresponding to the $B_u(\nu)$ oscillator when $q = 1,3$ and corresponding to the $A_g(\nu)$ oscillator when $q = 2$ and the normalization factor is $T^{(q)} = \sum_\nu |\tilde{p}_\nu^{(q)}|$. Calculations were made for the frequency of the peak $f(\hbar\omega = 1.97$ eV$)$.
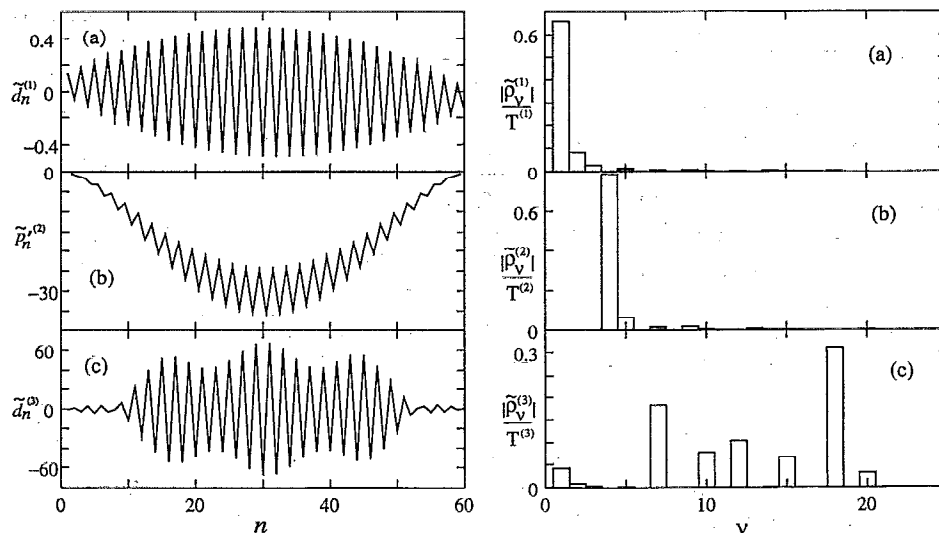
FIG. 8. Same as Fig. 7 except that the frequency is $\hbar\omega = 1.63$ eV (peak d).

is no unique dominant component, and many oscillators contribute to the density matrix in third order. In spite of the strong interferences among oscillators, we clearly see collective CDW like (charge density) fluctuations in the third order. The large first order charge density fluctuations at this frequency makes second order bond order parameter oscillations as well as the third order charge density fluctuations large, which results in the peak g in THG. We thus conclude that this peak is the single-photon resonance corresponding to the absorption peak A.

We next consider the density matrix at the frequency $\hbar\omega = 1.63$ eV. In first order, although the frequency is off resonance with respect to $B_u(1)$, this oscillator is dominant and its characteristic charge density distribution is clearly seen. This is because the oscillator strength of $B_u(1)$ is much larger than all other oscillators, so that it is

mainly excited even at off-resonance frequencies. Because of the off-resonance excitation, the charge density amplitude induced by the external field is much smaller compared with the single-photon resonant frequency $\hbar\omega = 1.97$ eV. In second order, the $A_g(4)$ oscillator is dominant. Moreover, the amplitude of bond order oscillations is comparable to that at the single-photon resonant frequency and much larger than for $\hbar\omega = 0.67$ eV. This indicates that the peak e is a two-photon resonance of $A_g(4)$. However, this peak is not at exactly half the frequency of $A_g(4)$ as seen from Fig. 6. The shift comes from the third order contributions as will be shown below. Half the frequency of $A_g(3)$ is closer to that of the peak e than the $A_g(4)$ oscillator. However, this oscillator with no bond order fluctuations is not excited, because of the Hamiltonian symmetry. One third the frequencies of the $B_u(16)-B_u(21)$
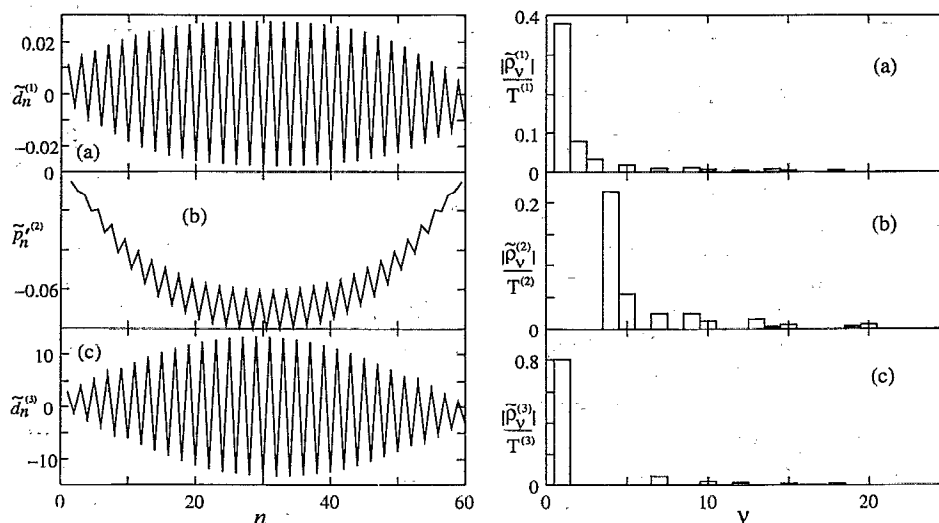
FIG. 9. Same as Fig. 7 except that the frequency is $\hbar\omega = 0.67$ eV (peak a).

oscillators are very close to the peak as seen from Fig. 6. However, from $|\tilde{p}_v^{(3)}|$ we see that many B_u oscillators contribute to the density matrix and the $B_u(16)-B_u(21)$ oscillators are not the dominant excitations. Therefore, the peak e cannot be identified as a three-photon resonance. However, because of the relatively large contribution of $B_u(18)$, the peak e is shifted from half the frequency of $A_g(4)$ towards one-third the frequency of $B_u(18)$. This illustrates the importance of interferences among oscillators.

Finally, we consider the density matrix at $\hbar\omega = 0.67$ eV. In the first (second) order, the amplitude of charge density (bond order) oscillation is much weaker than that at the single(two)-photon resonant frequency discussed above. Therefore, this is not a purely single- or two-photon resonance. Although $B_u(1)$ in first order and $A_g(4)$ in second order have relatively large contributions, this is also because of the huge oscillator strength of $B_u(1)$ and strong coupling between $B_u(1)$ and $A_g(4)$. In third order, the $B_u(1)$ component is dominant, and the amplitude of the charge density oscillation is comparable to those at the other two frequencies. Moreover, peak a is precisely at one-third the frequency of $B_u(1)$. We, therefore, conclude that the peak a in THG is the three-photon resonance corresponding to the absorption peak A. In this way, we can identify all the resonances in the THG spectrum.

In summary, we have made the following identifications: (i) peak b comes from three-photon resonance to $B_u(3)$ (corresponding to the absorption peak C); (ii) peak c is a three-photon resonance to $B_u(7)$ (corresponding to the absorption peak E); (iii) peak d is a three-photon resonance to $B_u(10)$ and $B_u(12)$. At this frequency, however, also $B_u(7)$ contributes to the density matrix significantly and they strongly interfere; (iv) peak f is a two-photon resonance to $A_g(5)$. However the contribution from $A_g(4)$ is the largest and these oscillators strongly interfere at this frequency. Using these results, we have identified the most important oscillators, namely, $B_u(1)$ with CDW like electronic structure and $A_g(4)$ with soliton pair like electronic structure. However, our analysis clearly shows that interference with the other oscillators cannot be neglected in the interpretation of the dispersed THG spectra.

Next, we compare the PPP and the Hückel results in Fig. 4 to illustrate the effect of Coulomb interaction. The following parameters which reproduce the experimentally observed energy gap of polyacetylene (2.0 eV) are used in the Hückel calculations: $U=0$, $\beta' = -4.4$ eV/Å, $K=20$ eV Å^{-2}. Other parameters are taken to be the same as for the PPP model. The TDHF Eq. (4.22) in the oscillator picture, shows the following two effects of Coulomb interaction. First, since the matrix $\mathscr{L}$ in the TDHF equation depends on γ_{mn}, the oscillators which diagonalize $\mathscr{L}$, are very different for the two models; few lowest frequency oscillators represent collective excitations in the PPP model. In contrast, the Hückel oscillators simply represent single electron-hole pairs. As can be seen from Figs. 2 and 4, these differences profoundly affect the absorption spectra; few lowest frequency collective oscillators carry almost the entire transition strength in the PPP model, whereas in

the Hückel model, the oscillator strength is much more uniformly distributed. Second, the Coulomb interaction strongly affects the coupling between oscillators. In particular, the anharmonic coupling [the last term in the right-hand side of Eq. (4.26), which couples the various RPA modes, takes into account correlation effects beyond the RPA approximation, or beyond configuration interaction with single electron hole pair states. The anharmonic coupling comes from Coulomb interactions, and it vanishes for the Hückel model where the only source of nonlinearity is the harmonic coupling among modes, induced by the external field (the second term in the right-hand side of Eq. (4.26)].

The Coulomb interaction strongly affects the dispersion of THG. In the Hückel model, all the major peaks $a,b,...,f$ in the THG spectra are simply three-photon resonances corresponding the $A,B,...,F$ peaks in the absorption spectra, as seen from Fig. 4. This is quite different for the PPP model.

Abe *et al.* have calculated THG spectra by summing over the excited states obtained by configuration interaction including only single electron-hole pair states.[15] Their calculation differs from ours mainly in the following two points. First, they used the Hückel ground state as opposed to the HF ground state in the present calculation. Therefore, their method is valid only when the Coulomb interaction is very weak. However, since exchange Coulomb interaction between adjacent sites, which stabilizes the BOW (HF ground state), can be incorporated via the renormalized Hückel parameters, this probably does not make a significant difference. Second, their method can describe collective excitations but does not take the nonlinear coupling between these collective excited states into account. Because of these differences, they obtained a very different dispersed THG spectrum. That calculation shows strongest peaks at the three-photon resonant frequency of the lowest frequency B_u exciton state, three-photon resonant peak of the conduction band edge, and two-photon resonant peak of the lowest frequency A_g exciton state. There is a direct correspondence between the first peak in both calculations but we find no analog to the other two resonances. This shows that the anharmonic couplings, which represent correlation effects beyond the RPA approximation, strongly affect the THG spectra.

The calculated TPA spectrum $\text{Im}[\gamma(-\omega;\omega,-\omega,\omega)]$ is displayed in Fig. 10. It shows a huge negative peak near the strongest absorption resonance and two weak positive peaks at the lower and higher energy sides of the peak. Since these peaks are close to the absorption peak, it is very difficult to resolve them experimentally. However, when we use parameters appropriate for polydiacetylene (stronger bond length alternation), the positive peak at the lower energy side shifts towards a lower energy, and the present theory can account for the experimental two-photon absorption spectrum of polydiacetylene. We also show the real and imaginary parts of the nonlinear optical polarizabilities connected to TPA and THG, and their phases defined by $\sin\phi = \text{Im}[\gamma]/|\gamma|$.[32] The phase provides a sensitive signature for the resonance structure.
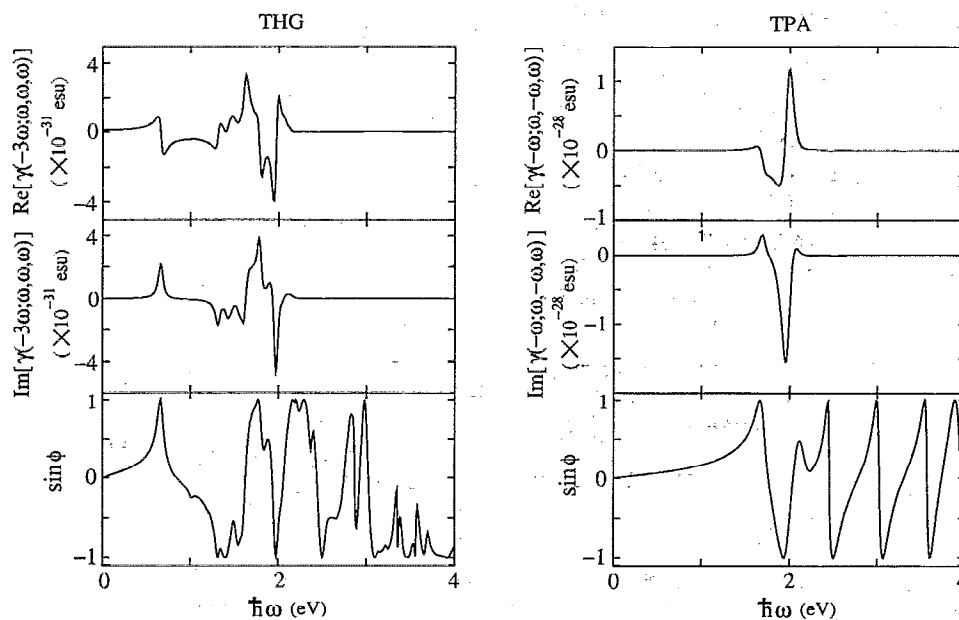
FIG. 10. The real part, the imaginary part and the phase $\sin \phi = \mathrm{Im}[\gamma]/|\gamma|$ of the third order nonlinear polarizabilities corresponding to third harmonic generation and two photon absorption are plotted vs ω for the PPP model.

VII. DISCUSSION

Starting with exact calculations of small size chains with up to 12 atoms, several authors argued that there are four essential states which almost dominate the nonlinear optics of π-conjugated polymers.[6] They are $1A_g$, $m A_g$, $1B_u$, and $n B_u$ states, where, $n A_g$ indicates the nth lowest energy A_g state, etc. The $1A_g$ state is the ground state and m and n depend on the system size. As indicated in the previous section, $B_u(1)$ makes a large contribution to the optical nonlinearity because it has a large oscillator strength, and $A_g(4)$ does contribute as well because it strongly couples with $B_u(1)$. Thus, the $B_u(1)$ and $A_g(4)$ oscillators correspond to the $1B_u$ and $m A_g$ excited states in the essential states picture. We found no oscillator clearly corresponding to the $n B_u$ state. However, since both $B_u(2)$ and $B_u(3)$ have a relatively large contribution, one of them may correspond to the $n B_u$ state. As indicated earlier, we cannot neglect the contributions from a large number of oscillators to the THG dispersion in our calculation. This is at variance with the essential states picture. There are several possible reasons for these differences. First, the oscillators in our picture are not just different ways of specifying excited states; the oscillators interfere and we can have resonances at the differences of their frequencies. When the interference is very strong (which is the case here), we cannot establish a clear one to one correspondence between oscillators and excited states. Second, the essential states picture is based on the calculation of short chains with at most 12 atoms. As seen from the electronic structure of the oscillators shown in Fig. 3, they have characteristic length scales much larger than 12 atoms. Therefore, in such short chains, the chain length strongly affects the electronic structure of the oscillators, as well as the corresponding nonlinear optical response.

Third, although some electron correlation effects beyond the RPA are taken into account, some of these effects cannot be described in our method. However, since the TDHF approximation used here can describe small amplitude collective fluctuations and their couplings very well, the approximation is particularly applicable to large systems, where collective motions are expected to be dominant.

We have taken the electron–phonon coupling into account in calculating the geometry optimized HF solution, but dynamical lattice motions were neglected in the present calculation. Since the mass of a carbon atom is much heavier than that of an electron, the effect of lattice motions is usually neglected. However, in the case of polyacetylene, the soliton mass is comparable to that of an electron,[33] and soliton like motions strongly affect the linear optics. Furthermore, Hagler and Heeger have argued using a simplified model that quantum lattice fluctuations significantly increase the off-resonant nonlinear optical susceptibilities.[7] This is an important subject for a future study. Note that it is straightforward to take the dynamics of lattice motions into account in our oscillator picture because this simply involves adding more oscillators to the model.

It is generally accepted that photoexcitation results in the formation of charged solitons.[33] A charged soliton has CDW like charge distribution around the soliton center.[34] Thus the characteristic charge distributions induced by the external field are very similar to those of a charged soliton. This suggests that these excitons may play some role in the decay process to charged solitons. This could be seen more directly using ultrafast four wave mixing spectroscopy, which will be studied in the future. Both in the present work and in Ref. 8, the nonlinear polarizabilities are calculated by solving equations of motion for the reduced

single electron density matrix, starting with the PPP model. However, the present approach has the following advantages: First, the site representation of the density matrix is used in this paper opposed to the Wannier function representation used in Ref. 8. Consequently, the present formalism can be applied to any geometry, and is not limited to periodic systems. In addition, various physical quantities such as the total dipole moment [Eq. (2.10)] can be represented very simply in the present formalism. Second, the zeroth order density matrix in the present paper is the HF solution as opposed to the Hückel ground state used in Ref. 8. We thus take the Coulomb interactions into account in the ground as well as in the excited states, whereas in Ref. 8 only excited state corrections were incorporated. Third, we have used a more systematic factorization based on a single, simple assumption (the TDHF approximation). The second term in Eq. (3.6) was neglected in Ref. 8 (the third term cancels out in the TDHF equation). The present formula can be applied also to other systems such as metal clusters.[35]

ACKNOWLEDGMENTS

APPENDIX A: GEOMETRY OPTIMIZED HARTREE–FOCK SOLUTION

In this appendix we outline the calculation of the HF solution. First, we assume a fixed geometry and a trial density matrix $\bar{\rho}''$ which is believed to be similar to the HF solution, and calculate the Fock operator $h[\bar{\rho}'']$. Then, by diagonalizing h, we obtain the molecular orbitals (MO) $|k\rangle \equiv \sum_n c_{nk}\hat{c}_n^\dagger |0\rangle$, whose coefficients c_{nk} satisfy

$$\sum_n h_{mn}c_{nk}=\epsilon_k c_{mk}, \tag{A1}$$

and ϵ_k are the HF energies. The coefficients satisfy the following orthonormality and closure relations

$$\sum_m c_{mk}c_{mk'}=\delta_{k,k'}, \tag{A2}$$

$$\sum_k c_{mk}c_{nk}=\delta_{m,n}. \tag{A3}$$

Using these coefficients, we construct the new density matrix $\bar{\rho}'$,

$$\sum_h^{occ} c_{mh}c_{nh}=\bar{\rho}'_{mn}, \tag{A4}$$

where the h summation is carried out over the occupied MO orbitals. From $\bar{\rho}'$, we obtain a new Fock operator, and repeat this process until the old and the new density matrices converge. The converged density matrix is the desired HF solution.

In order to calculate the geometry optimized HF solution, the geometry x_n should satisfy the force equilibrium condition

$$\frac{\partial\langle|H|\rangle}{\partial x_n}=0, \tag{A5}$$

where $|\rangle$ is the HF wave function and $n=1,...,N-1$. Using Hellman–Feynmann theorem, Eq. (A5) can be recast as

$$\left\langle\left|\frac{\partial H}{\partial x_n}\right|\right\rangle=0. \tag{A6}$$

From Eqs. (2.4), (2.5), and (A6), the force equilibrium condition assumes the form

$$K(x_n-\bar{x})-4\beta'\bar{\rho}_{n,n+1}=0. \tag{A7}$$

To calculate the geometry optimized HF solution, we first assume a trial x_n which are believed to be similar to the geometry optimized HF solution, and calculate the HF solution for this fixed geometry. Next we calculate new x_n which satisfy the force equilibrium condition with the HF solution from Eq. (A7), and then calculate the HF solution with this new geometry. By repeating this process until the old and the new x_n converge, we finally obtain the geometry optimized HF solution.

APPENDIX B: HARTREE–FOCK, MOLECULAR ORBITAL, AND HARMONIC OSCILLATOR REPRESENTATIONS

We first introduce the HFMO representation. Using the orthogonality and closure properties of the HF orbitals (A2) and (A3), we obtain

$$\mathscr{V}^{-1}=\mathscr{V}^T. \tag{B1}$$

Thus,

$$\delta\rho_{mn}=\sum_{kk'}\mathscr{V}_{kk',mn}\delta\rho_{kk'}. \tag{B2}$$

Substituting Eq. (B2) into the TDHF Eq. (4.40) in the real space representation, and multiplying this equation by $\mathscr{V}$ from the left-hand side, we obtain the TDHF equation in the HFMO representation. Using Eq. (B1), we can easily show that the TDHF equation in the HFMO representation is given by Eq. (4.14).

Substituting Eq. (4.17) into Eq. (4.8), we obtain

$$i\hbar\dot{\delta\rho}_1-[\bar{h},\delta\rho_1]-[\delta h_1,\bar{\rho}]$$
$$=[f,\bar{\rho}]+[f,\delta\rho]+[\bar{h},\delta\rho_2]+[\delta h_2,\bar{\rho}]+[\delta h,\delta\rho], \tag{B3}$$

$$i\hbar\dot{\delta\rho}_2-[\bar{h},\delta\rho_2]-[\delta h_2,\bar{\rho}]$$
$$=[f,\bar{\rho}]+[f,\delta\rho]+[\bar{h},\delta\rho_1]+[\delta h_1,\bar{\rho}]+[\delta h,\delta\rho]. \tag{B4}$$

Transforming these TDHF equations from the real space to the HFMO representation as shown to derive Eq. (4.14) and using the fact that the eh and he components of $[\bar{h},\delta\rho_2]$, and the ee' and hh' components of $[f,\bar{\rho}]$, $[\bar{h},\delta\rho_1]$, and $[\delta h_1,\bar{\rho}]$ vanish, we obtain Eqs. (4.18) and (4.19). Here the $M_1\times M_1$ HF stability matrix $\mathscr{L}_1$ is given by

$$\mathscr{L}_{1eh,e'h'} = (\epsilon_e - \epsilon_h)\delta_{e,e'}\delta_{h,h'} + \widetilde{\gamma}_{ehe'h'},$$

$$\mathscr{L}_{1eh,h'e'} = \widetilde{\gamma}_{ehh'e'},$$

$$\mathscr{L}_{1he,e'h'} = -\mathscr{L}_{1e'h',he}, \tag{B5}$$

$$\mathscr{L}_{1he,h'e'} = -\mathscr{L}_{1eh,e'h'},$$

where

$$\widetilde{\gamma}_{kk'k_1k_2} = \sum_{mn} \mathscr{V}_{kk',mm}\mathscr{V}_{k_1k_2,nn}\gamma_{mn}. \tag{B6}$$

The $M_2 \times M_2$ matrix Ω_2 is diagonal in Liouville space and its matrix elements are given by

$$(\Omega_2)_{ee',ee'} = (\epsilon_e - \epsilon_{e'}),$$

$$(\Omega_2)_{hh',hh'} = (\epsilon_h - \epsilon_{h'}), \tag{B7}$$

where ϵ_k is the HF energy of HF orbital k. Note that $\Omega_{2ee'ee'} = -\Omega_{2e'e,e'e}$ and $\Omega_{2hh',hh'} = -\Omega_{2h'h,h'h}$.

We next turn to the HO representation. As shown in Ref. 22, $\mathscr{L}_1$ can be diagonalized by matrix w,

$$w\mathscr{L}_1 w^{-1} = \Omega_1. \tag{B8}$$

The matrix w can be expressed using the $M_1/2 \times M_1/2$ matrices X and Y as

$$w = \begin{bmatrix} X & -Y \\ Y & -X \end{bmatrix}, \tag{B9}$$

which implies that

$$w_{v,eh} = X_{v,eh},$$

$$w_{v,he} = -Y_{v,eh},$$

$$w_{\bar{v},eh} = Y_{v,eh}, \tag{B10}$$

$$w_{\bar{v},he} = -X_{v,eh},$$

where $\Omega_{1\,v} > 0$ and $\Omega_{1\,\bar{v}} = -\Omega_{1\,v}$. The matrix w^{-1} can be written as

$$w^{-1} = \begin{bmatrix} X^T & -Y^T \\ Y^T & -X^T \end{bmatrix}. \tag{B11}$$

The matrices X and Y were obtained by a numerical diagonalization of $\mathscr{L}_1$ [Eq. (B8)].

We next rewrite the TDHF equation using the HO representation. The third term on the right-hand side of Eq. (4.8) is transformed to the HO representation by

$$[\delta h, \delta\rho]_v = \sum_{mn} \mathscr{U}_{v,mn}[\delta h, \delta\rho]_{mn}. \tag{B12}$$

Substituting Eq. (4.7) and

$$\delta\rho_{mn} = \sum_v \mathscr{U}_{mn,v}^{-1}\delta\rho_v, \tag{B13}$$

into Eq. (B12), we obtain

$$[\delta h, \delta\rho]_v = \sum_{mnlv'v''} \mathscr{U}_{v,mn}(\gamma_{ml} - \gamma_{nl})(2\mathscr{U}_{ll,v'}^{-1}\mathscr{U}_{mn,v''}^{-1}$$
$$- \mathscr{U}_{ml,v'}^{-1}\mathscr{U}_{ln,v''}^{-1})\delta\rho_{v'}\delta\rho_{v''}. \tag{B14}$$

In the same way, the first and second terms are given by

$$[f,\bar{\rho}]_v = \sum_{mnl} \mathscr{U}_{v,mn}(f_{ml}\bar{\rho}_{ln} - f_{ln}\bar{\rho}_{ml}), \tag{B15}$$

$$[f,\delta\rho]_v = \sum_{mnlv'} \mathscr{U}_{v,mn}(f_{ml}\mathscr{U}_{ln,v'}^{-1} - f_{ln}\mathscr{U}_{ml,v'}^{-1})\delta\rho_{v'}. \tag{B16}$$

Therefore, the TDHF equation assumes the form of Eq. (4.26), where

$$F_v = \sum_{mnl} \mathscr{U}_{v,mn}(f_{ml}\bar{\rho}_{ln} - f_{ln}\bar{\rho}_{ml}), \tag{B17}$$

$$G_{v,v'} = \sum_{mnl} \mathscr{U}_{v,mn}(f_{ml}\mathscr{U}_{ln,v'}^{-1} - f_{ln}\mathscr{U}_{ml,v'}^{-1}), \tag{B18}$$

$$R_{v,v'} = \sum_{mnl} \mathscr{U}_{v,mn}[2(\gamma_{ml} - \gamma_{nl})\bar{\rho}_{mn}\mathscr{U}_{ll,v'}^{-1} - \gamma_{ml}\bar{\rho}_{ln}\mathscr{U}_{ml,v'}^{-1}$$
$$+ \gamma_{nl}\bar{\rho}_{ml}\mathscr{U}_{ln,v'}^{-1}], \tag{B19}$$

$$S_{v,v'v''} = \sum_{mnlv'} \mathscr{U}_{v,mn}(\gamma_{ml} - \gamma_{nl})(2\mathscr{U}_{ll,v'}^{-1}\mathscr{U}_{mn,v''}^{-1}$$
$$- \mathscr{U}_{ml,v'}^{-1}\mathscr{U}_{ln,v''}^{-1}). \tag{B20}$$

APPENDIX C: SOLUTION OF THE TIME DEPENDENT HARTREE–FOCK EQUATION

The density matrix obtained from the TDHF equation, when written in the TDHF MO basis has the following form at all times (Note that this matrix is identical to the single electron reduced density matrix except for the normalization, its trace is equal to half the number of electrons n and is not equal to 1).

$$\rho(t) = \begin{bmatrix} I & 0 \\ 0 & 0 \end{bmatrix}. \tag{C1}$$

It is then clear that this density matrix is a projection operator which satisfies

$$\rho(t)^2 = \rho(t). \tag{C2}$$

Here we regard ρ as an $N \times N$ matrix (rather than a vector in Liouville space). Note that although the complete many body density matrix $|\psi(t)\rangle\langle\psi(t)|$ represents a pure state, this is not the case for the single particle density matrix ρ. Nevertheless, Eq. (C2) holds because of the special form of ρ. Substituting Eq. (4.4) into Eq. (C2), we obtain

$$\delta\rho(t) = \delta\rho(t)\bar{\rho} + \bar{\rho}\delta\rho(t) + \delta\rho(t)^2. \tag{C3}$$

In the HFMO representation, the HF solution is given by

$$\bar{\rho}_{hh'} = \delta_{h,h'},$$

$$\bar{\rho}_{ee'} = 0. \tag{C4}$$

Substituting Eqs. (C4) into Eq. (C3), we obtain

$$\delta\rho(t)_{hh'} = -\sum_k \delta\rho(t)_{hk}\delta\rho(t)_{kh'}, \tag{C5}$$

$$\delta\rho(t)_{ee'} = \sum_k \delta\rho(t)_{ek} \delta\rho(t)_{ke'}. \tag{C6}$$

When the expansion of $\delta\rho$ in powers of the external field Eq. (5.1) is substituted in Eqs. (C5) and (C6), and performing a Fourier transform to the frequency domain, we obtain

$$\rho(\omega)_{hh'}^{(1)} = 0, \tag{C7a}$$

$$\rho(\omega)_{ee'}^{(1)} = 0, \tag{C7b}$$

$$\rho(\omega)_{hh'}^{(2)} = -\frac{1}{\sqrt{2\pi}} \int_{-\infty}^{\infty} \sum_k \rho(\omega')_{hk}^{(1)} \rho(\omega-\omega')_{kh'}^{(1)} d\omega', \tag{C8a}$$

$$\rho(\omega)_{ee'}^{(2)} = \frac{1}{\sqrt{2\pi}} \int_{-\infty}^{\infty} \sum_k \rho(\omega')_{ek}^{(1)} \rho(\omega-\omega')_{ke'}^{(1)} d\omega', \tag{C8b}$$

$$\rho(\omega)_{hh'}^{(3)} = -\frac{1}{\sqrt{2\pi}} \int_{-\infty}^{\infty} \sum_k [\rho(\omega')_{hk}^{(1)} \rho(\omega-\omega')_{kh'}^{(2)}$$
$$+ \rho(\omega')_{hk}^{(2)} \rho(\omega-\omega')_{kh'}^{(1)}] d\omega', \tag{C9a}$$

$$\rho(\omega)_{ee'}^{(3)} = \frac{1}{\sqrt{2\pi}} \int_{-\infty}^{\infty} \sum_k [\rho(\omega')_{ek}^{(1)} \rho(\omega-\omega')_{ke'}^{(2)}$$
$$+ \rho(\omega')_{ek}^{(2)} \rho(\omega-\omega')_{ke'}^{(1)}] d\omega'. \tag{C9b}$$

Similarly, we can calculate $\rho_2^{(q)}$ from $\rho^{(q-1)},...,\rho^{(1)}$ without solving the TDHF equation directly. However, the TDHF equations are required in order to calculate ρ_1.

Next, we consider $\rho_1^{(q)}$. Substituting Eq. (5.1) into Eq. (4.18) and using Eq. (4.21), we obtain for the TDHF equation for the first order in the HO representation

$$(\hbar\omega + i\Gamma)\rho_1{}^{(1)}_\nu(\omega) - \Omega_1{}_\nu\rho_1{}^{(1)}_\nu(\omega) = [f(\omega),\bar{\rho}]_\nu, \tag{C10a}$$

where we added the damping term and Γ is the damping constant. We obtain $\rho_1^{(1)}$ from this closed equation. The second and third order density matrices obtained in the same way as

$$(\hbar\omega + i\Gamma)\rho_1{}^{(2)}_\nu(\omega) - \hbar\Omega_1{}_\nu\rho_1{}^{(2)}_\nu(\omega)$$
$$= [h_2^{(2)}(\omega),\bar{\rho}]_\nu + \frac{1}{\sqrt{2\pi}} \int_{-\infty}^{\infty} \{[h^{(1)}(\omega'),\rho^{(1)}(\omega-\omega')]_\nu$$
$$+ [f(\omega'),\rho^{(1)}(\omega-\omega')]_\nu\} d\omega', \tag{C10b}$$

$$(\hbar\omega + i\Gamma)\rho_1{}^{(3)}_\nu(\omega) - \hbar\Omega_1{}_\nu\rho_1{}^{(3)}_\nu(\omega)$$
$$= [h_2^{(3)}(\omega),\bar{\rho}]_\nu + \frac{1}{\sqrt{2\pi}} \int_{-\infty}^{\infty} \{[h^{(1)}(\omega'),\rho^{(2)}(\omega-\omega')]_\nu$$
$$+ [h^{(2)}(\omega'),\rho^{(1)}(\omega-\omega')]_\nu$$
$$+ [f(\omega'),\rho^{(2)}(\omega-\omega')]_\nu\} d\omega'. \tag{C10c}$$

We can calculate $\rho_1^{(q)}$ from $\rho_2^{(q)}$ and lower order density matrices using Eqs. (C10). In this way, we can calculate density matrices to the arbitral order.

Finally, we derive the Drude formula for linear absorption. The qth order polarization $P^{(q)}$ can be expressed using the density matrix in the HFMO representation

$$P^{(q)}(\omega) = -2e \sum_{eh} z_{eh}[\rho_{eh}^{(q)}(\omega) + \rho_{he}^{(q)}(\omega)], \tag{C11}$$

where

$$z_{kk'} = \sum_n V_{kk',nn} z(n). \tag{C12}$$

Using the matrices X and Y, the first order solution of the TDHF Eq. (C10a) can also be represented in the HFMO basis. Substituting the solution into Eq. (C11), we obtain Eqs. (6.5) and (6.6).

APPENDIX D: OPTICAL SUSCEPTIBILITIES AND CHARGE DENSITY FLUCTUATIONS

In this appendix we review the basic definitions of nonlinear optical polarizabilities and relate them to our equations of motion.

We first consider the following single mode optical electric field:

$$E(t) = E_1 \cos \omega_1 t. \tag{D1}$$

Performing a Fourier transformation, we obtain

$$E(\omega) = \sqrt{\frac{\pi}{2}} E_1 \delta(\omega-\omega_1) + \sqrt{\frac{\pi}{2}} E_1 \delta(\omega+\omega_1). \tag{D2}$$

Substituting Eq. (D2) into Eq. (3.9), we get

$$f(\omega) = \tilde{f}(\omega_1)\delta(\omega-\omega_1) + \tilde{f}(-\omega_1)\delta(\omega+\omega_1), \tag{D3}$$

where

$$\tilde{f}_{mn}(\pm\omega_1) = \sqrt{\frac{\pi}{2}} \delta_{m,n} ez(n)E_1. \tag{D4}$$

Substituting Eq. (D3) into Eq. (5.8a), results in

$$\rho^{(1)}(\omega) = \tilde{\rho}^{(1)}(\omega_1;-\omega_1)\delta(\omega+\omega_1)$$
$$+ \tilde{\rho}^{(1)}(-\omega_1;\omega_1)\delta(\omega-\omega_1), \tag{D5}$$

where

$$\tilde{\rho}^{(1)}(\mp\omega_1;\pm\omega_1) = \mathscr{G}(\pm\omega_1)[f(\pm\omega_1),\bar{\rho}]. \tag{D6}$$

Equation (D5) together with Eq. (5.8b) yield

$$\rho^{(2)}(\omega) = \tilde{\rho}^{(2)}(2\omega_1;-\omega_1,-\omega_1)\delta(\omega+2\omega_1)$$
$$+ \tilde{\rho}^{(2)}(0;-\omega_1,\omega_1)\delta(\omega) + \tilde{\rho}^{(2)}(-2\omega_1;\omega_1,\omega_1)$$
$$\times \delta(\omega-2\omega_1). \tag{D7}$$

$\tilde{\rho}^{(2)}$ is given by

$\widetilde{\rho}^{(2)}(\mp 2\omega_1;\pm\omega_1,\pm\omega_1)$

$$= \frac{1}{\sqrt{2\pi}}\,\mathscr{G}(\pm 2\omega_1)\{[\widetilde{h}^{(1)}(\mp\omega_1;\pm\omega_1),$$

$$\widetilde{\rho}^{(1)}(\mp\omega_1;\pm\omega_1)]+[\widetilde{f}(\pm\omega_1),$$

$$\widetilde{\rho}^{(1)}(\mp\omega_1;\pm\omega_1)]\},\qquad \text{(D8a)}$$

$\widetilde{\rho}^{(2)}(0;-\omega_1,\omega_1)$

$$= \frac{1}{\sqrt{2\pi}}\,\mathscr{G}(0)\{[\widetilde{h}^{(1)}(-\omega_1;\omega_1),\widetilde{\rho}^{(1)}(\omega_1;-\omega_1)]$$

$$+[\widetilde{h}^{(1)}(\omega_1;-\omega_1),\widetilde{\rho}^{(1)}(-\omega_1;\omega_1)]+[\widetilde{f}(\omega_1),$$

$$\widetilde{\rho}^{(1)}(\omega_1;-\omega_1)]+[\widetilde{f}(-\omega_1),\widetilde{\rho}^{(1)}(-\omega_1;\omega_1)]\},$$

$$\text{(D8b)}$$

where we define $\widetilde{h}^{(1)}(-\omega_1;\omega_1)$ by the following equation:

$$\widetilde{h}_{nm}^{(1)}(-\omega_1;\omega_1)=2\delta_{n,m}\sum_l \gamma_{nl}\widetilde{\rho}_{ll}^{(1)}(-\omega_1;\omega_1)$$

$$-\gamma_{nm}\widetilde{\rho}_{nm}^{(1)}(-\omega_1;\omega_1)\qquad \text{(D9)}$$

[other $\widetilde{h}^{(q)}$ with different frequencies and with different orders, are defined in the same way).

Substituting Eqs. (D5), (D7), and (D9) into Eq. (5.8c), we obtain

$$\rho^{(3)}(\omega)=\widetilde{\rho}^{(3)}(3\omega_1;-\omega_1,-\omega_1,-\omega_1)\delta(\omega+3\omega_1)$$

$$+\widetilde{\rho}^{(3)}(\omega_1;-\omega_1,-\omega_1,\omega_1)\delta(\omega+\omega_1)$$

$$+\widetilde{\rho}^{(3)}(-\omega_1;\omega_1,\omega_1,-\omega_1)\}\delta(\omega-\omega_1)$$

$$+\widetilde{\rho}^{(3)}(-3\omega_1;\omega_1,\omega_1,\omega_1)\delta(\omega-3\omega_1),\quad \text{(D10)}$$

where

$$\widetilde{\rho}^{(3)}(\mp 3\omega_1;\pm\omega_1,\pm\omega_1,\pm\omega_1)=\frac{1}{\sqrt{2\pi}}\,\mathscr{G}(\pm 3\omega_1)\{[\widetilde{h}^{(1)}(\mp\omega_1;\pm\omega_1),\widetilde{\rho}^{(2)}(\mp 2\omega_1;\pm\omega_1,\pm\omega_1)]$$

$$+[\widetilde{h}^{(2)}(\mp 2\omega_1;\pm\omega_1,\pm\omega_1),\widetilde{\rho}^{(1)}(\mp\omega_1;\pm\omega_1)]+[\widetilde{f}(\pm\omega_1),\widetilde{\rho}^{(2)}(\mp 2\omega_1;\pm\omega_1,\pm\omega_1)]\},$$

$$\text{(D11a)}$$

$$\widetilde{\rho}^{(3)}(\mp\omega_1;\pm\omega_1,\pm\omega_1,\mp\omega_1)=\frac{1}{\sqrt{2\pi}}\,\mathscr{G}(\pm\omega_1)\{[\widetilde{h}^{(1)}(\mp\omega_1;\pm\omega_1),\widetilde{\rho}^{(2)}(0;\pm\omega_1,\mp\omega_1)]+[\widetilde{h}^{(1)}(\pm\omega_1;\mp\omega_1),$$

$$\widetilde{\rho}^{(2)}(\mp 2\omega_1;\pm\omega_1,\pm\omega_1)]+[\widetilde{h}^{(2)}(\mp 2\omega_1;\pm\omega_1,\pm\omega_1),\widetilde{\rho}^{(1)}(\pm\omega_1;\mp\omega_1)]$$

$$+[\widetilde{h}^{(2)}(0;\pm\omega_1,\mp\omega_1),\widetilde{\rho}^{(1)}(\mp\omega_1;\pm\omega_1)]+[\widetilde{f}(\pm\omega_1),\widetilde{\rho}^{(2)}(0;\pm\omega_1,\mp\omega_1)]$$

$$+[\widetilde{f}(\mp\omega_1),\widetilde{\rho}^{(2)}(\mp 2\omega_1;\pm\omega_1,\pm\omega_1)]\},$$

$$\text{(D11b)}$$

and so forth. Performing the inverse Fourier transformation of Eq. (D10) with Eqs. (D11), we obtain

$$\rho^{(3)}(t)=\frac{1}{\sqrt{2\pi}}\,[\widetilde{\rho}^{(3)}(-3\omega_1;\omega_1,\omega_1,\omega_1)\exp(3i\omega_1 t)+\widetilde{\rho}^{(3)}$$

$$\times(-\omega_1;\omega_1,\omega_1,-\omega_1)\exp(i\omega_1 t)+\text{h.c.}],\quad \text{(D12)}$$

where the relation

$$[\rho^{(q)}]^{\dagger}(\omega)=\rho^{(q)}(-\omega),\qquad \text{(D13)}$$

has been used.

The optical polarizabilities are defined using the total polarization $P(t)$ of a single molecule

$$P^{(1)}(t)=\frac{1}{2}[\alpha(-\omega_1;\omega_1)\exp(i\omega_1 t)+\text{c.c.}]E_1,\qquad \text{(D14a)}$$

$$P^{(3)}(t)=\frac{1}{2}\,[\gamma(-3\omega_1;\omega_1,\omega_1,\omega_1)\exp(3i\omega_1 t)$$

$$+\gamma(-\omega_1;\omega_1,-\omega_1,\omega_1)\}\exp(i\omega_1 t)+\text{c.c.}]E_1^3,$$

$$\text{(D14b)}$$

where $\alpha(-\omega;\omega)$ is the linear polarizability and $\gamma(-3\omega;\omega,\omega,\omega)$ and $\gamma(-\omega;\omega,-\omega,\omega)$ are third-order optical polarizabilities connected to THG and TPA, respectively. Note that this definition is the same as the common definition in the off-resonant frequency region, where the imaginary parts of the polarizabilities vanish. Comparing Eqs. (D14) with Eqs. (5.11) and (D12), we obtain Eqs. (5.12) and (5.13).

[1] *Nonlinear Optical Properties of Organic and Polymeric Materials*, edited by D. J. Williams (American Chemical Society, Washington, 1983), Series 233.

[2] *Nonlinear Optical Effects in Organic Polymers*, NATO Advanced Study Institute, Series E, edited by J. Mrssier, F. Kajzar, P. N. Prasad, and D. R. Ulrich (Kluwer Academic, Dordrecht, 1989), Vol. 162.

[3] *Nonlinear Optical Properties of Organic Molecules and Crystals*, edited by D. S. Chemla and J. Zyss (Academic, New York, 1987).

[4] *Nonlinear Optical and Electroactive Polymers*, edited by P. N. Prasad and D. Ulrich (Plenum, New York, 1988).

[5] *Nonlinear Optical Properties of Polymers*, edited by A. J. Heeger, J. Orenstein, and D. R. Ulrich (MRS, Pittsburg, 1988), Vol. 109.

[6] S. Etemad and Z. G. Soos, in *Spectroscopy of Advanced Materials*, edited by R. J. H. Clark and R. E. Hester (Wiley, New York, 1991), pp. 87, and references therein.

[7] T. W. Hagler and A. J. Heeger, Chem. Phys. Lett. 189, 333 (1992).

[8] S. Mukamel and H. X. Wang, Phys. Rev. Lett. 69, 65 (1992); H. X. Wang and S. Mukamel, J. Chem. Phys. 97, 8019 (1992).

[9] B. J. Orr and J. F. Ward, Mol. Phys. 20, 513 (1971).

[10] B. Kirtman, Int. J. Quantum Chem. 43, 147 (1992).

[11] G. P. Agrawal, C. Cojan, and C. Flyzanis, Phys. Rev. B 16, 776 (1978).

[12] W. K. Wu, Phys. Rev. Lett. 61, 1119 (1988).

[13] J. Yu et al., Phys. Rev. B 39, 12 814 (1989).

[14] X. Sun, K. Nasu, and C. Q. Wu, Appl. Phys. B 54, 170 (1992).

[15] S. Abe, M. Schreiber, W. P. Su, and J. Yu, Chem. Phys. Lett. 192, 425 (1992); S. Abe, M. Schreiber, W. P. Su, and J. Yu, Phys. Rev. B 45, 9432 (1992).

[16] I. Ohmine and M. Karplus, J. Chem. Phys. 68, 2298 (1978); K. Schulten, I. Ohmine, and M. Karplus, ibid. 64, 4422 (1976); G. J. B. Hurst, M. Dupuis, and E. Clementi, ibid. 89, 385 (1989).

[17] S. R. Marder, J. W. Perry, G. Bourhill, C. B. Gorman, and B. G. Tieman, Science 261, 186 (1993); S. M. Risser, D. N. Beratan, and S. R. Marder, J. Am. Chem. Soc. 115, 7719 (1993).

[18] U. Fano, Rev. Mod. Phys. 29, 74 (1957).

[19] N. Bloembergen, Nonlinear Optics (Benjamin, New York, 1965).

[20] F. C. Spano and S. Mukamel, Phys. Rev. Lett. 66, 1197 (1991); Phys. Rev. A 40, 5783 (1989).

[21] S. Mukamel, in Molecular Nonlinear Optics, edited by J. Zyss (Academic, New York, 1994), p. 1.

[22] A. F. Garitos, J. R. Heflin, F. Y. Wong, and Q. Zamani-Khamiri, in Organic Materials for Nonlinear Optics, Special Publication No. 69, edited by R. A. Hann and D. Bloor (Royal Society of Chemistry, London, 1988); J. R. Heflin, K. Y. Wong, Q. Zamani-Khamiri, and A.

F. Garito, Phys. Rev. B 38, 157 (1988); Mol. Cryst. Liq. Cryst. 160, 37 (1988).

[23] H. Fukutome, J. Mol. Struct. (Theochem) 188, 337 (1989); and references therein.

[24] Z. G. Soos, in Electroresponsive and Polymeric Systems, edited by T. A. Marcel (Dekker, New York, 1988), Vol. 1.

[25] D. Yaron and R. J. Silbey, Phys. Rev. B 45, 11655 (1992).

[26] P. Ring and P. Schuck, The Nuclear Many-Body Problem (Springer, New York, 1980).

[27] See, for example, H. Sekino and R. J. Bartlett, J. Chem. Phys. 94, 3665 (1991); 98, 3022 (1993).

[28] A. Stahl and I. Balslev, Electrodynamics of the Semiconductor Band Edge (Springer, Berlin, Heidelberg, 1987).

[29] S. Mukamel, J. Chem. Phys. 93, 1 (1982).

[30] W. S. Fann, S. Benson, J. M. Madey, S. Etemad, G. L. Baker, and F. Kajzar, Phys. Rev. Lett. 62, 1492 (1989).

[31] C. Halvorson, T. W. Hagler, D. Moses, Y. Cao, and A. J. Heeger, Chem. Phys. Lett. 200, 364 (1992).

[32] W. E. Torruellas, D. Neher, R. Zanoni, G. I. Stegeman, and F. Kajzar, Chem. Phys. Lett. 175, 11 (1990); W. E. Torruellas, K. B. Rochford, R. Zanoni, S. Aramaki, and G. I. Stegeman, Opt. Commun. 82, 94 (1991); S. Aramaki, W. Torruellas, R. Zanoni, and G. I. Stegeman, ibid. 85, 527 (1991).

[33] A. J. Heeger, S. Kivelson, J. R. Schrieffer, and W. P. Su, Rev. Mod. Phys. 60, 781 (1988), and references therein.

[34] H. Fukutome and M. Sasai, Prog. Theor. Phys. 69, 373 (1983).

[35] V. B. Koutecky, P. Fantucci, and J. Koutecky, Chem. Rev. 91, 1035 (1991).